Electrochemical Reducation of TiO2/Al2O3/C to Ti3AlC2 and Its Derived Two-Dimensional (2D) Carbides

Li, Shangshu; Zou, Xingli; Hu, Yong; Lu, Xionggang; Xiong, Xiaolu; Xu, Qian; Cheng, Hongwei; Zhou, Zhongfu

Published in:
Journal of the Electrochemical Society

DOI:
10.1149/2.0181803jes

Publication date:
2018

Citation for published version (APA):
Li, S., Zou, X., Hu, Y., Lu, X., Xiong, X., Xu, Q., Cheng, H., & Zhou, Z. (2018). Electrochemical Reducation of TiO2/Al2O3/C to Ti3AlC2 and Its Derived Two-Dimensional (2D) Carbides. *Journal of the Electrochemical Society*, *165*(3), E97-E107. https://doi.org/10.1149/2.0181803jes

Electrochemical reduction of $TiO_2/Al_2O_3/C$ to Ti_3AlC_2 and its derived two-dimensional (2D) carbides

Shangshu Li,[a] Xingli Zou,[a,b,*] Yong Hu,[a] Xionggang Lu,[a,*] Xiaolu Xiong,[a] Qian Xu,[a] Hongwei Cheng,[a] and Zhongfu Zhou[a,c]

a. State Key Laboratory of Advanced Special Steel & Shanghai Key Laboratory of Advanced Ferrometallurgy & School of Materials Science and Engineering, Shanghai University, Shanghai 200072, China

b. Center for Electrochemistry, Department of Chemistry, The University of Texas at Austin, Austin, Texas 78712, USA

c. Institute of Mathematics and Physics, Aberystwyth University, Aberystwyth, SY23 3BZ, UK

*Corresponding author, E-mail: xzou@utexas.edu (X. Zou), luxg@shu.edu.cn (X. Lu)

Abstract

Ti_3AlC_2 has been directly synthesized from $TiO_2/Al_2O_3/C$ mixture precursors ($3TiO_2/0.5Al_2O_3/1.5C$ and $2TiO_2/0.5Al_2O_3/C$) by a molten salt electrolysis process at 900 °C and 3.2 V in molten $CaCl_2$. The influence of initial carbon content on the electrosynthesized products has been investigated. The result shows that the main phase of the electrosynthesized products changes from Ti_3AlC to Ti_2AlC and then to Ti_3AlC_2 with the increasing carbon content, and the electrosynthesized Ti_3AlC_2 is carbon deficient. The morphology observation shows that the electrosynthesized Ti_3AlC_2 particles possess smooth surfaces and dense flake-like microstructure. The reaction mechanism of the electroreduction of $TiO_2/Al_2O_3/C$ mixture precursor has

been discussed based on the time- and position-dependent phase constitution analysis. In addition, two-dimensional (2D) Ti_3AlC_2-derived carbides, *i.e.*, $Ti_3C_2T_x$ and TiC_x have been successfully prepared from the electrosynthesized Ti_3AlC_2 by a chemical etching process and an electrochemical etching process, respectively. Both derived carbides exhibit the similar layered structure, in which single layer carbides are composed of plentiful nanometer carbides. It is suggested that the molten salt electrolysis process has a great potential to be used for the facile synthesis of $M_{n+1}AX_n$ phases (such as Ti_3AlC_2) from their oxides precursors, and the synthesized $M_{n+1}AX_n$ phases can be further converted into 2D carbides.

Keywords: Ti_3AlC_2; Electroreduction; $TiO_2/Al_2O_3/C$ precursors; Molten $CaCl_2$; Two-dimensional carbides

1. Introduction

Ternary intermetallic $M_{n+1}AX_n$ phases (M presents an early transition metal, A presents a III/IV-group element, X is C or N, and n = 1–3) possess many excellent properties of both ceramic and metal owing to their peculiar layered structure and the mixed metallic-covalent bonds nature [1, 2]. It is well known that $M_{n+1}AX_n$ phases mainly include three groups, *i.e.*, M_2AX, M_3AX_2 and M_4AX_3, depending on *n* values [3]. Among the M_3AX_2 groups, Ti_3AlC_2 has been extensively investigated by researchers due to its unique merits, such as low density (4.247 g/cm^3), high strength, excellent thermal conductivity, good oxidation resistance, and irradiation resistance [4-8]. Therefore, Ti_3AlC_2 has been considered as a promising candidate for high-temperature applications, such as fuel cladding materials for fission/fusion

reactors [8]. Generally, various methods including self-propagating high-temperature synthesis (SHS), hot pressing (HP), pulse discharge sintering (PDS), *etc.* can be used to prepare Ti_3AlC_2 from pure metals (Ti/Al/C), carbides (TiC_x/Al or Ti/Al_4C_3/TiC), and hydride (TiH_2/Al/C) [4, 9-17]. However, these processes are commonly performed under severe conditions, such as high temperature and high pressure. Furthermore, the conventional production of pure metals (such as Ti) usually suffers from the energy-intensive and tedious process. Therefore, a simple and green method with low cost is needed to prepare Ti_3AlC_2.

Molten salt electrolysis process is a potential candidate technology for the facile synthesis of $M_{n+1}AX_n$ phases under moderate conditions [18]. This method employs the simple oxides as cathode precursor and graphite rod (or inert anode) as an anode. During the molten salt electrolysis process, oxygen is first ionized at the cathode, dissolved in the molten salt electrolyte and then discharged at the anode [19]. Ultimately, oxygen will react with carbon to generate CO or CO_2 gas at the anode, and the other elements will *in situ* interact with each other to form alloys or composites at the cathode [20]. More detailed features of the molten salt electrolysis process can be found in elsewhere [21, 22]. Until now, many metals (such as Ti, Si, Ge), alloys (such as TiC, Ti_5Si_3), and composites (such as Fe-TiC, Ti_5Si_3-TiC) have been successfully synthesized by the molten salt electrolysis process [22-27]. In addition, the direct electroreduction of solid Al_2O_3 has also been investigated in different molten salts, such as $CaCl_2$-NaCl, $CaCl_2$-LiCl, and $CaCl_2$-CaF_2 [28-30]. Noteworthily, Al has a low melting point of 660 °C, which means that formed Al is

liquid when the electrolysis was carried out at a higher temperature (such as 900 °C). In order to overcome this drawback, the mixed oxides can be used as the precursor to directly synthesize refractory alloys, such as Ti-6Al-4Al [21].

Two-dimensional (2D) materials, such as graphene and MoS_2, have attracted extensive attention in the past decade. These materials usually possess remarkable electronic, mechanical and optical properties that are different from their 3D counterparts [31, 32]. Two approaches can be used in general to produce 2D materials. One is the physical process, such as the exfoliation of graphite. Another is the selective extraction process (such as the preparation of 2D transition metal carbides), which is based on the difference in stability/reactivity between the different components of the corresponding 3D counterparts [31]. Ti_3AlC_2 can be used as the precursor to prepare 2D transition metal carbides by the selective extraction process. It is well known that Ti_3AlC_2 has a layered hexagonal structure which consists of edge-shared Ti_6C octahedra interleaved with pure Al layers [2, 3]. In Ti_3AlC_2, Al layers are more reactive because they are relatively weakly bonded compared with the Ti-C bonds [33]. Therefore, Al layers can be easily extracted from Ti_3AlC_2. The previous work has demonstrated that 2D transition metal carbides, named MXenes (such as $Ti_3C_2T_x$ (T = –OH or –F/=O)), can be prepared from $M_{n+1}AX_n$ phases (such as Ti_3AlC_2) by the chemical etching method [33-36]. MXenes possess excellent properties, such as good electronic conductivity and high corrosion resistance, which enable a wide range of potential applications [37-39].

In the present work, we first aimed to synthesize Ti_3AlC_2 from $TiO_2/Al_2O_3/C$

precursor by molten salt electrolysis process in molten $CaCl_2$. The influence of the precursor compositions on final electrosynthesized products was investigated. The current feature and phase constitution of the products during the electrolysis were analyzed. The final products were characterized, and the reaction mechanism of the electroreduction process was discussed based on the experimental results. Afterwards, for the extended application of the electrosynthesized Ti_3AlC_2, the synthesized Ti_3AlC_2 was further converted into two-dimensional (2D) carbides, *i.e.*, $Ti_3C_2T_x$ (T = –OH or –F/=O) and TiC_x, through a subsequent chemical and electrochemical etching processes respectively on the basis of the selective extraction of Al layers, as illustrated in Figure 1. These two kinds of derived carbides were also characterized and analyzed.

2. Experimental

2.1 Fabrication of the electrodes

The electrolytic cell was composed of the oxides/carbon mixture cathode, the graphite anode, and molten $CaCl_2$ (≥99.0 %) as electrolyte contained in a corundum crucible. Commercially available TiO_2 (25 nm, 99.8 %), Al_2O_3 (~18 μm, 99.5 %) and carbon (30 nm, 99.5 %) powders were used as precursors. TiO_2, Al_2O_3, and C were firstly mixed at the corresponding stoichiometric ratio (Ti:Al:C = 3:1:*x* (*x* = 0.2–2.0) and 2:1:1), and then ball milled with 5 wt % polyvinyl butyral (PVB) in anhydrous alcohol for 5 h. PVB was used as the binder and it would easily volatilize at the experimental temperature. Approximately 0.5 g of the milled mixture was pressed under a stable pressure of 12 MPa in a die to form a cylindrical pellet with a diameter

of 10 mm. Finally, the pressed pellet without sintering was wrapped with two pieces of porous nickel foils (~95 % porosity) and fixed by a Fe-Cr-Al alloy wire to form a cathode. The nickel foil can provide many contact points to the pellet's surface and thus benefit to the electroreduction of oxides during the initial stage of the electrolysis. A high-purity graphite rod with a diameter of 12 mm was used as the anode, and a Fe-Cr-Al alloy wire was tied to the graphite rod to conduct current.

2.2 Electroreduction process and etching experiment

The electroreduction process was performed in a sealed corundum reactor located inside a vertical electrical furnace. High purity argon gas was continuously introduced into the reactor to maintain an inert atmosphere during the electrolysis. The electrolysis was carried out at 900 °C and 3.2 V between the $TiO_2/Al_2O_3/C$ mixture cathode and the graphite anode. It is suggested that carbon cannot directly react with TiO_2 and/or Al_2O_3 at 900 °C based on the thermodynamic calculation, *i.e.*, $TiO_2 + C = TiO + CO$ (ΔG^θ = 86.164 kJ/mol); $TiO_2 + 2C = Ti + 2CO$ (ΔG^θ = 301.145 kJ/mol); $TiO_2 + 3C = TiC + 2CO$ (ΔG^θ = 129.785 kJ/mol); $Al_2O_3 + 3C = 2Al + 3CO(g)$ (ΔG^θ = 657.094 kJ/mol). Before the electrolysis, a pre-electrolysis with aim to eliminate residual moisture and redox-active species from molten $CaCl_2$ was conducted at 2.5 V between the Mo wire cathode and graphite anode. A Biologic HCP-803 electrochemical workstation was used to control the electroreduction process and record the corresponding current-time curve. After the electrolysis experiment was terminated and the furnace was cooled to room temperature, the cathode was taken out from solidified $CaCl_2$ by dissolving the salt in flowing tap

water. The obtained electrodeoxidized pellet was then washed with distilled water to remove the residual $CaCl_2$ and dried at 50 °C in a drying oven.

In addition, two etching processes including chemical etching and electrochemical etching were carried out respectively to prepare 2D carbides from the electrosynthesized Ti_3AlC_2. For the chemical etching (*i.e.*, preparation of $Ti_3C_2T_x$), the obtained Ti_3AlC_2 was firstly ground to powder and then immersed in 40 % concentrated HF solution at room temperature for 24 h (Figure 1). After the immersing process, the reaction product was washed with deionized water until the PH is around 7.0 and dried in vacuum. For the electrochemical etching (*i.e.*, preparation of TiC_x), the etching process was carried out at 900 °C and 2.5 V for 24 h between a graphite cathode and the Ti_3AlC_2 anode in molten $CaCl_2$ (Figure 1). After the electrochemical etching process, the collection process of samples is same as the above-mentioned electroreduction process.

2.3 Characterization of the products

The oxygen content of the products was measured by the oxygen analyzer (TC-436, LECO, America). The phase constitution of the products was characterized by a X-ray diffractometer (XRD) with Cu $K\alpha_1$ radiation (D8 ADVANCE, Bruker, Germany) and a Raman spectrometer with 523 nm laser beam (LabRam HR 800, Horiba Jobin Yvon, France) in a backscattering configuration at ambient temperature. The structure of $Ti_3C_2T_x$ was also identified by the Fourier transform infrared (FTIR) spectrometer (TENSOR 27, Bruker Optik GmbH, Germany). The morphology of the products was examined by the scanning electron microscopy (SEM, JEOL

JSM-6700F, Japan) and the corresponding element composition was analyzed by the energy dispersive X-ray spectrometer (EDS, Oxford INCA EDS system) attached to the SEM. Additionally, the microstructure of the products was further investigated by using a high-resolution transmission electron microscopy (HRTEM, FEI TF20, Holland) with an acceleration voltage of 200 kV.

3. Results and discussion

3.1 Electrosynthesis of Ti_3AlC_2 from $3TiO_2/0.5Al_2O_3/xC$ precursors

3.1.1 Various precursor compositions and the variation of current

The influence of the precursor compositions on the final electrosynthesized products was first investigated. TiO_2 and Al_2O_3 contents were kept fixed in the precursors, and the stoichiometry range was set as Ti_3AlC_x where x = 0.2–2.0. The oxygen content of the products is approximately 3800 ppm (an average of oxygen contents of all products) after 22 h electrolysis, which indicates that the products with low oxygen contents can be obtained according to the electroreduction process. As summarized in Table 1, the phase constitutions of the final products obtained from the electrolysis of 22 h are various as the initial carbon contents are changed. Additionally, the main phases show a tendency of $Ti_3AlC \rightarrow Ti_2AlC \rightarrow Ti_3AlC_2$ with the increase of carbon content. It should be noted that the product mainly includes Ti_3AlC_2, $TiAl_3$ and TiC when the precursor composition is $3TiO_2/0.5Al_2O_3/2C$ (*i.e.*, stoichiometric ratio of Ti:Al:C = 3:1:2). The relatively pure Ti_3AlC_2 can be obtained from the $3TiO_2/0.5Al_2O_3/1.5C$ (*i.e.*, stoichiometric ratio of Ti:Al:C = 3:1:1.5) precursor. In fact, Ti_3AlC_2 has been found to be carbon deficient with respect to its ideal stoichiometry

in the previous work [40], and the influence of carbon content on the preparation of Ti_3AlC_2 by using the conventional methods has also been investigated [9, 41, 42].

Figure 2 shows the current-time curve of the electroreduction process of the $3TiO_2/0.5Al_2O_3/1.5C$ precursor. As shown in the figure, the current variation can be divided into two stages, *i.e.*, the rapid decline and the slow decline. The current starts at a higher level of around 2.30 A and rapidly decreases to approximately 1.00 A within 2 h electrolysis. This observation is mainly attributed to the reduction of the pellet's surface, which is relatively kinetic favorable during the early stage of the electrolysis [26, 43]. The porous nickel foils can also provide many initial reduction points to the pellet's surface. Subsequently, the decline of the current becomes slower because of the increasing reduction kinetics restriction. The mass/oxygen ions transfer in the pellet's inner part is slower due to the hindering of the formed metal/alloy layers [23, 44]. Therefore, the reduction of the pellet's inner part is relatively slower compared with that of the pellet's outer part. When oxides/compounds (such as TiO_2, Al_2O_3, $CaTiO_3$ and $Ca_{12}Al_{14}O_{33}$, see Figure 3) are gradually reduced, the current finally decreases to approximately 3.80 A (residual current) during the later stage of the electrolysis. The total charge passed through the electrolytic cell is around 13.1 Ah within 22 h electrolysis. The current efficiency is defined as the percentage of the theoretical charge for reducing all oxides (TiO_2 and Al_2O_3) and the actual charge (*i.e.*, total charge passed through the electrolytic cell), which can be obtained from the integration of current-time curve. The current efficiency of the electroreduction process is calculated to be approximately 17.9 %. After the electrolysis experiment,

some carbon powders cover on the solidified $CaCl_2$. The lower current efficiency is mainly ascribed to the influence of carbon powder dropped from the graphite anode or formed through the side reaction ($CO_3^{2-} + 4e^- = C + 3O^{2-}$) [21, 22, 27]. The previous work has reported that the dropped/formed carbon powder could immerse into the electrolyte and then influence the electronic conductivity of the molten salt, which will inevitably reduce the current efficiency [27]. A modified anode, such as solid oxide membrane (SOM)-based anode, can be used as an inert anode to improve the current efficiency [27, 44].

3.1.2 The changes of phase constitution

Generally, the electroreduction process for oxides in molten salt is a complicated process, which includes the oxygen-ions transfer process and the *in-situ* interaction of the elements, *etc.* [24] These processes always result in the phase change during the electrolysis. The interrupted experiments can be used to investigate the changes of phase constitution. It is evident that the oxides (TiO_2 and Al_2O_3) and carbon are gradually transformed into Ti_3AlC_2, as presented in Figure 3. Intermediate phases TiC_mO_n, $Ca_{12}Al_{14}O_{33}$ (PDF# 48-1882), $CaTiO_3$ (PDF# 89-6949), as well as unreacted TiO_2 (PDF# 83-2242) and Al_2O_3 (PDF# 78-2426) coexist in the product obtained from 1 h electrolysis. $Ca_{12}Al_{14}O_{33}$ and $CaTiO_3$ are usually formed through reactions (1) and (2), which typically involves the incorporation of CaO/($Ca^{2+} + O^{2-}$) into the pellet [24, 25, 45], *i.e.*, the interaction between CaO/($Ca^{2+} + O^{2-}$) and Al_2O_3 as well as TiO_2, respectively. CaO may inevitably exist in molten $CaCl_2$ due to the impurity of purchased $CaCl_2$ and the hydrolysis reaction ($CaCl_2 \cdot H_2O = CaO + 2HCl$) [24].

$7Al_2O_3 + 12CaO/(Ca^{2+} + O^{2-}) = Ca_{12}Al_{14}O_{33}$ $\Delta G^{\theta} = -351.503$ kJ/mol (1)

$TiO_2 + CaO/(Ca^{2+} + O^{2-}) = CaTiO_3$ $\Delta G^{\theta} = -87.627$ kJ/mol (2)

When prolonging the electrolysis time to 2.5–5 h, a certain amount of Al_2O_3 still exists in the pellet (Figure 3), and no TiO_2 is found. It is suggested that Al_2O_3 (decomposition voltage is 2.25 V ($Al_2O_3 = 2Al + 1.5O_2$)) is more stable than TiO_2 (decomposition voltage is 1.31 V ($4TiO_2 = Ti_4O_7 + 0.5O_2$)) during the electroreduction process. After being electrolyzed for 2.5 h, Ti_3AlC_2 (PDF# 52-0875) begins to form and the characteristic peaks of Ti_3AlC_2 gradually accrete with the increasing electrolysis time. In addition, the compounds/oxides (*i.e.*, TiC_mO_n, $Ca_{12}Al_{14}O_{33}$, $CaTiO_3$ and Al_2O_3) are gradually reduced as the electroreduction process proceeds (such as electrolysis of 5–7.5 h). Among these intermediate phases, the reduction of $Ca_{12}Al_{14}O_{33}$ is relatively difficult due to the higher decomposition voltage (2.34 V ($2Ca_{12}Al_{14}O_{33} = 24CaO + 28Al + 21O_2$)). As shown in Figure 3, besides Ti_3AlC_2 and TiC_mO_n, the product obtained from electrolysis of 7.5 h still contains a small amount of $Ca_{12}Al_{14}O_{33}$. Main phase Ti_3AlC_2 (along with a trace amount of TiC_x and Ti_3Al (PDF# 52-0859)) is finally formed when the electrolysis time is extended to 10–22 h. The ICP analysis gives an atom ratio of Ti:Al = 74.53:25.47 in the final product, which is close to the initial molar ratio of Ti:Al = 3:1. This observation indicates that the formed Al can react immediately with other intermediate products to form high melting phase, although the melting point of Al (660 °C) is lower than the experimental temperature (900 °C).

It should be noted that TiC_mO_n can be considered as a kind of solid solution of

titanium monoxide (TiO) and titanium carbide (TiC) [46-48], and the generated TiC_mO_n may accelerate the electroreduction process due to its good electronic conductivity. In addition, the stoichiometry of TiC_mO_n will vary with the gradual removal of oxygen as well as the incorporation of C element during the electroreduction process (reaction (3)) [26, 49]. A careful analysis of XRD patterns reveals that the (111) and (200) peaks of TiC_mO_n shift gradually to lower angels with the increase of electrolysis time, as shown in Figure 4a and b. This observation indicates that the lattice parameter of TiC_mO_n has changed. The lattice parameter of TiC_mO_n usually increases from 4.194 (pure TiO) to 4.325 Å (pure TiC) with the reduction of TiC_mO_n (reaction (3)) [46, 49]. In this work, the lattice parameters are 4.307, 4.313, 4.319 and 4.320 Å as the pellet is electrolyzed for 1, 2.5, 5 and 7.5 h, respectively (Figure 4c). Noteworthily, the lattice parameter of the final product (such as 10 and 22 h) is 4.330 Å, which may be attributed to the formation of carbon-deficient TiC (marked as TiC_x) and the influence of Al element according to the previous work [50]. Actually, TiC_x generally exhibits a wide range of stoichiometry ($x \geq 0.47$) without any crystal structure change [51].

$$TiC_mO_n + (1-m)C + 2ne^- = TiC + nO^{2-} \quad (3)$$

Besides the above time-dependent phase analysis, the position-dependent phase analysis can also be used to investigate the detailed phase change. In this experiment, the partially reduced pellets were first ground from its surface to center in a certain distance (approximately 0.3 mm), and then the phase constitution of the ground pellets was determined by XRD. Figure 5a presents the XRD pattern of the pellet

obtained from the 2 h electrolysis. It can be seen from the figure that the phase constitution seems to have no obvious changes, and the phases include Ti_2O_3 (PDF# 71-0281), TiC_mO_n, $Ca_{12}Al_{14}O_{33}$, Al_2O_3 and $CaTiO_3$ at all layers of the pellet. This observation indicates that the electrolysis process mainly includes the reduction of TiO_2 and the formation of TiC_mO_n, $Ca_{12}Al_{14}O_{33}$, as well as $CaTiO_3$ during the early stage of the electrolysis. During the electroreduction process, O^{2-} is generated from the reduction of oxides (such as $2TiO_2 + 2e^- = Ti_2O_3 + O^{2-}$). The generated O^{2-} and Ca^{2+} would further react with Al_2O_3 and TiO_2 to form $Ca_{12}Al_{14}O_{33}$ and $CaTiO_3$ in molten $CaCl_2$, respectively. as discussed in reactions (1) and (2). In addition, the formation of TiC_mO_n mainly involves the electroreduction process and the carbonization process, as described in reactions (4) and (5).

$$CaTiO_3 + mC + 2(2-n)e^- = TiC_mO_n + CaO + (2-n)O^{2-} \quad (4)$$

$$Ti_2O_3 + 2mC + 2(3-2n)e^- = 2TiC_mO_n + (3-2n)O^{2-} \quad (5)$$

Figure 5b shows the XRD pattern of the pellet obtained from the 5 h electrolysis. It is obvious that the product of the pellet's surface consists of Ti_3AlC_2, Ti_2AlC (PDF# 29-0095) and TiC_mO_n. However, besides these phases, $Ca_{12}Al_{14}O_{33}$ still exists in the product of the pellet's interior part. It is suggested that the electroreduction of the oxides/compounds and the formation of Ti_3AlC_2 occur at the pellet's surface and gradually proceeds along the depth direction. In addition, the peak intensities of Ti_2AlC and TiC_mO_n gradually decrease along the depth direction from the pellet's center to its surface (Figure 5b and c). Therefore, according to these experimental results (Figures 3 and 4) and the above discussions, the formation of Ti_3AlC_2 may

follow the sequence of TiC_mO_n, $Ca_{12}Al_{14}O_{33}$ → TiC, Ti_2AlC → Ti_3AlC_2. The previous works were confirmed that TiC can react with Ti_2AlC to form Ti_3AlC_2 (TiC + Ti_2AlC → Ti_3AlC_2), and a possible reaction mechanism has been proposed [52, 53].

3.1.3 Microstructure observation

Figure 6a and b show the SEM images of the obtained product electrolyzed for 22 h. As revealed in Figure 6a, the electrosynthesized Ti_3AlC_2 particles have smooth surfaces and typically possess a flake-like microstructure. In addition, some smaller particles have interconnected with each other to form larger particles, as shown in Figure 6b. This observation is mainly due to the sintering of the formed Ti_3AlC_2 particles at the experimental temperature (900 °C) during the later stage of the electrolysis. The TEM images of the obtained Ti_3AlC_2 are presented in Figure 6c and d. In Figure 6c, it can be found that Ti_3AlC_2 has the layered structure. The lattice fringes of the electrosynthesized Ti_3AlC_2 are clearly visible in Figure 6d, and the interplanar spacing of 9.145 Å can be identified as *d*(002) of Ti_3AlC_2. In addition, the lattice parameters of the electrosynthesized Ti_3AlC_2 are calculated to be a = 3.07 Å and c = 18.30 Å by the Rietveld refinement using TOtal PAttern Solution (TOPAS) software. According to the following formula (*eq.* (6)), the calculated *d*(002) is 9.15 Å, which is close to the above experimental value. In fact, the lattice parameters of Ti_3AlC_2 always vary with the distinction of experiment conditions [4, 54-58], which may be attributed to the carbon-deficient structure of Ti_3AlC_2.

$$d_{(hkl)}=\frac{1}{\sqrt{\frac{4\left(h^2+hk+k^2\right)}{3a^2}+\frac{l^2}{c^2}}} \quad (6)$$

3.2 Electrosynthesis of Ti_3AlC_2 from $2TiO_2/0.5Al_2O_3/C$ precursors

3.2.1 Current feature and phase constitution changes

Besides $3TiO_2/0.5Al_2O_3/1.5C$ precursor, the $2TiO_2/0.5Al_2O_3/C$ precursor was also used to prepare Ti_3AlC_2 for comparison in molten $CaCl_2$ at 900 °C and 3.2 V. Figure 7 shows the current-time curve of the electroreduction process for the $2TiO_2/0.5Al_2O_3/C$ precursor. The current variation reflects a tendency of the first rapid decline and then slow decline, which is similar to the electroreduction process of the $3TiO_2/0.5Al_2O_3/1.5C$ precursor. The decrease of current during the electroreduction of the $2TiO_2/0.5Al_2O_3/C$ precursor is more slower compared with that of the $3TiO_2/0.5Al_2O_3/1.5C$ precursor. Additionally, the residual current (approximately 4.20 A) is higher than that of the electrolysis of $3TiO_2/0.5Al_2O_3/1.5C$ precursor (around 3.80 A). This observation suggests that the precursor composition (*i.e.*, different precursors) can influence the current features during the electrolysis. The total charge passed through the electrolytic cell is around 21.9 Ah, and the current efficiency is calculated to be approximately 12.9 %. It should be noted that the current efficiency can be influenced by many factors, such as porosity of the pellet and the particle sizes of the feed materials [59].

Figure 8 presents the XRD patterns of the products obtained from the $2TiO_2/0.5Al_2O_3/C$ pellets after being electrolyzed for different times. It can be found that the product is composed of $Ca_{12}Al_{14}O_{33}$, $CaTiO_3$, Al_2O_3, Ti_4O_7 (PDF# 50-0787) and Ti_3O_5 (PDF# 40-0806) after 4 h electrolysis. Besides $Ca_{12}Al_{14}O_{33}$, $CaTiO_3$ and Al_2O_3, TiC_mO_n and Ti_2O_3 also coexist in the product after being electrolyzed for 8 h. It is suggested that the reduction of TiO_2 is a multistep process, *i.e.*, $TiO_2 \rightarrow Ti_4O_7 \rightarrow$

$Ti_3O_5 \rightarrow Ti_2O_3$ (*i.e.*, $4TiO_2 + 2e^- = Ti_4O_7 + O^{2-}$, $3Ti_4O_7 + 2e^- = 4Ti_3O_5 + O^{2-}$, and $2Ti_3O_5 + 2e^- = 3Ti_2O_3 + O^{2-}$). Ti_3AlC_2 begins to form after electrolysis for 12 h, and the intermediate compounds $Ca_{12}Al_{14}O_{33}$, TiC_mO_n and Al_2O_3, are gradually reduced with the increasing electrolysis time. Main phase Ti_3AlC_2 and a trace amount of TiC_x and $TiAl_3$ (PDF# 65-0429) are identified as the final products obtained from the electrolysis of 22 h. Similar to the electroreduction of $TiO_2/Al_2O_3/1.5C$, the lattice parameter of TiC_mO_n solid solution increases with the increasing electrolysis time. As shown in Figure 9, the lattice parameters of TiC_mO_n are 4.306, 4.318 and 4.322 Å after electrolysis for 4, 8, and 12 h, respectively. The lattice parameter of TiC_x is 4.330 Å after electrolysis for 16–24 h. In addition, the lattice parameters of the electrosynthesized Ti_3AlC_2 from $2TiO_2/0.5Al_2O_3/C$ precursor are calculated to be a = 3.07 Å and c = 18.41 Å, which are different from the lattice parameters of Ti_3AlC_2 obtained from the $3TiO_2/0.5Al_2O_3/1.5C$ precursor. It is suggested that the element compositions (Ti, Al and C contents) can influence the crystal structure of the electrosynthesized Ti_3AlC_2.

In addition, Ti_3AlC_2 phase has also been identified by Raman spectroscopy. Figure 10 shows the Raman spectrum of the product obtained from 22 h electrolysis. The spectrum corresponding to Ti_3AlC_2 typically exhibits major Raman peaks at 185.0, 203.3, 273.3, 632.2 and 662.1 cm^{-1}. These six peaks correspond to the six Raman active first-order vibrations, *i.e.*, $2E_{2g} + 2E_{1g} + 2A_{1g}$ [60]. The peaks at 185.0, 203.3 and 273.3 cm^{-1} are attributed to the vibrations of Al atoms, and the peaks at 632.2 and 660.1 cm^{-1} are ascribed to the vibrations of C atoms in Ti_3AlC_2 [61].

3.2.2 Morphology observation

It is well known that the three-phases interlines (3PIs) reaction mechanism can be used to describe the electroreduction of solid oxide pellets [62]. A partially reduced pellet (electrolyzed for 8 h) can be used to confirm the 3PIs reaction process. The partially reduced pellet was first ground to the centre, and the section of the pellet was then analyzed by backscattered electron (BSE) analysis. As shown in Figure 11a, the BSE image of the section of the pellet exhibits two different colors, *i.e.*, gray and white. The corresponding element mapping analysis (Figure 11b-f, the brightness in element mapping corresponds to the abundance of element) reveals that the pellet's outer part mainly consists of elements Ti, Al and C, and the inner part mainly includes elements Ti, Al, C, Ca and O. This observation suggests that the reduction of the pellet starts at the surface and end up at the centre. In addition, according to the XRD analysis (Figure 8), the pellet's outer part (gray) is mainly composed of Ti_3AlC_2 and $TiAl_3$, and the pellet's inner part (white) largely includes $Ca_{12}Al_{14}O_{33}$, Al_2O_3 and TiC_mO_n.

Figure 12a shows the SEM image of the product obtained from 4 h electrolysis. It is obvious that the product possesses heterogeneous and coarse morphologies. The EDS analysis shows that elements Ti, Al, Ca, O and C coexist in the pellet. Therefore, according to the XRD analysis (Figure 8), it is suggested that the heterogeneous and coarse morphologies correspond to the coexistence of $Ca_{12}Al_{14}O_{33}$, Al_2O_3, $CaTiO_3$, Ti_3O_5, Ti_4O_7 and C. It should be noted that the presence of Pt peaks in EDS spectra is due to the coating used for the SEM and EDS analyses (the same below). When these

oxides/compounds are gradually reduced and Ti_3AlC_2 was finally formed, the product possesses the smooth surface and flake-like microstructure (Figure 12b). Like Ti_3AlC_2 prepared from the $3TiO_2/0.5Al_2O_3/1.5C$ precursor (Figure 6b), the obtained Ti_3AlC_2 particles synthesized from the $2TiO_2/0.5Al_2O_3/C$ precursor also interconnect with each other owing to the sintering of the particles. In addition, according to the EDS analysis, it is also indicated that elements Ca and O have been completely removed from the pellet after electrolysis for 22 h.

3.3 The reaction mechanism of the electroreduction of $TiO_2/Al_2O_3/C$ precursor

In summary, a multi-step reaction mechanism including the formation of the intermediate compounds (*i.e.*, $Ca_{12}Al_{14}O_{33}$, $CaTiO_3$ and TiC_mO_n), the reduction of the intermediate compounds, and the formation of Ti_3AlC_2 is proposed based on the above experimental results and the previous work [24, 26, 45, 46, 53]. $Ca_{12}Al_{14}O_{33}$ and $CaTiO_3$ are formed through the interaction of CaO/(Ca^{2+} + O^{2-}) and Al_2O_3 as well as TiO_2 respectively, as described in reactions (1) and (2). It should be noted that the migrations of O^{2-} actually go through a cyclic process, in which O^{2-} is firstly generated from the reduction of oxides (such as TiO_2, Ti_4O_7 and Ti_3O_5) and then incorporated with Ca^{2+} into pellet during the early stage of the electrolysis. $CaTiO_3$ and Ti_2O_3 are then partially reduced and react *in-situ* with C to form TiC_mO_n according to reactions (4) and (5). TiC_mO_n will be continually reduced and simultaneously react immediately with C and Al (generated from the reduction of $Ca_{12}Al_{14}O_{33}$ and Al_2O_3 [28] (reactions (7) and (8)) to form Ti_2AlC according to reaction (9). Finally, the generated Ti_2AlC will immediately react with the residual

TiC to form Ti_3AlC_2 according to reaction (10).

$$Ca_{12}Al_{14}O_{33} + 42e^- = 14Al + 12CaO + 21O^{2-} \quad (7)$$

$$Al_2O_3 + 6e^- = 2Al + 3O^{2-} \quad (8)$$

$$3TiC_mO_n + Al + (2\text{-}3m)C + 6ne^- = TiC + Ti_2AlC + 3nO^{2-} \quad (9)$$

$$TiC + Ti_2AlC = Ti_3AlC_2 \quad (10)$$

It is worth noting that both the generated CaO (reactions (4) and (7)) and Ca (generated from the reduction of CaO) can readily dissolve into molten $CaCl_2$ [63, 64]. Therefore, element Ca would be easily removed from the pellet during the electroreduction process. Additionally, it should be noted that Ca can accelerate the reduction process through the calciothermic reaction, *i.e.*, $M_xO_y + yCa = yCaO + xM$ (M presents metals) [64-66] and the dissolution of CaO in molten $CaCl_2$.

3.4 Preparation of Ti_3AlC_2-derived two-dimensional (2D) carbides

In this work, we have also investigated the preparation of $Ti_3C_2T_x$ from the electrosynthesized Ti_3AlC_2 by the chemical etching process, as illustrated in Figure 1. In addition, we tried to *in-situ* prepare the layered carbide (TiC_x) from the electrosynthesized Ti_3AlC_2 through an electrochemical etching process (Figure 1) based on the selective extraction of Al layers in Ti_3AlC_2.

3.4.1 Preparation of $Ti_3C_2T_x$ from the electrosynthesized Ti_3AlC_2

Figure 13a shows the XRD patterns of the products before and after the chemical etching process (immersing in 40 % HF solutions), respectively. It is obvious that the strong peaks of Ti_3AlC_2 disappear and the characteristic peaks of $Ti_3C_2T_x$ appear after being immersed for 24 h. The peaks detected at 2θ = 9.076 and 18.353° are attributed

420 to $Ti_3C_2F_2$, and the peak of 2θ = 27.796° corresponds to the formation of $Ti_3C_2(OH)_2$
421 [67]. During the etching process, Al layers are firstly selectively etched ($2Ti_3AlC_2$ +
422 $6HF = 2Ti_3C_2 + 2AlF_3 + 3H_2$) because the weaker bonding between Ti and Al. The
423 replaceable groups, such as –OH and –F, are then attached to the exposed Ti atoms of
424 the generated Ti_3C_2 surface (Figure 1b), *i.e.*, $Ti_3C_2 + 2H_2O = Ti_3C_2(OH)_2 + H_2$, and
425 $Ti_3C_2 + 2HF = Ti_3C_2F_2 + H_2$ [33]. The prepared $Ti_3C_2T_x$ particles (average particle
426 size is ~ 300 nm) exhibits a loose multilayered structure, which differs from the
427 closely aligned layered Ti_3AlC_2 precursor, as shown in Figures 13b and 6a.
428 Additionally, the thickness (cross section in Figure 13b) of the multilayer-structured
429 particles is approximately 200 nm. Interestingly, each layer of the $Ti_3C_2T_x$ is
430 composed of many minisize $Ti_3C_2T_x$ particles, and it may be due to the pulverization
431 of individual Ti_3C_2 sheets according to the previous work [34]. No element Al exists
432 in the immersed product according to the EDS analysis, suggesting that the Al layers
433 (in Ti_3AlC_2) have been completely etched. The existence of elements F and O also
434 demonstrates that the surface of Ti_3C_2 has been terminated by F/O-containing grounds
435 (such as -F and -OH).

436 In order to further determine the surface structure, the obtained $Ti_3C_2T_x$ was
437 analyzed by FTIR spectrometer, as revealed in Figure 13c. The adsorption peaks
438 detected at ~1051, ~1101 and ~1384 cm^{-1} are attributed to the existence of C–O, C–F
439 and O–H groups, respectively [68]. In addition, the peaks at ~1628 and ~3437 cm^{-1}
440 indicate the presence of hydroxyl groups on the surface of $Ti_3C_2T_x$. The peak at ~615
441 cm^{-1} corresponds to the deformation vibration for the Ti–O bond [67, 69]. Therefore,

based on the FTIR analysis, it is confirmed that the surface of $Ti_3C_2T_x$ is terminated by =O, –OH and –F groups. Figure 13d shows the TEM image of the cross-section of the $Ti_3C_2T_x$. It can be seen from the figure that $Ti_3C_2T_x$ sheets show an accordion-like stacked morphology, which consists of many lamellar $Ti_3C_2T_x$. It should be noted that the single-/few- layered $Ti_3C_2T_x$ can be prepared by the delamination treatment (usually upon sonication) [33]. The corresponding selected area electron diffraction (SAED, the inset in Figure 13d) of $Ti_3C_2T_x$ exhibits the diffuse dim spots, which typically correspond to the hexagonal symmetry [70]. It is suggested that the obtained $Ti_3C_2T_x$ sheets remain a hexagonal crystal structure.

3.4.2 *In-situ* preparation of TiC_x from the electrosynthesized Ti_3AlC_2

Besides $Ti_3C_2T_x$, we have also tried to prepare the layered TiC_x for the first time from the electrosynthesized Ti_3AlC_2 through an electrochemical etching process based on the extractable feature of Al layers from Ti_3AlC_2 (Figure 1). In the experiment, the commercial Ti_3AlC_2 (~74 μm, ≥98.5 %, obtained from Forsman Ltd., Beijing) was first used as the anode precursor, the graphite rod was served as the cathode, and the molten $CaCl_2$ contained in corundum crucible was employed as electrolyte. Figure 14a shows the XRD patterns of the commercial Ti_3AlC_2 before and after 24 h electrochemical etching at 900 °C and 2.5 V. It can be seen from the XRD patterns that the peaks of Ti_3AlC_2 have completely disappeared after 24 h electrochemical etching process. The characteristic peaks of new phase are identified as TiC_x. The commercial Ti_3AlC_2 possesses the coarse layered morphology due to the mechanical grinding, as shown in Figure 14b. After 24 h electrochemical etching, the obtained

464 TiC_x retains the layered structure, which is similar to the microstructure of Ti_3AlC_2
465 precursor, as revealed in Figure 14c. In addition, the magnified SEM image in Figure
466 14d shows that the obtained TiC_x sheets are stacked by many single layered TiC_x, and
467 the single-layered TiC_x is composed of plentiful nanometer TiC_x particles. It should be
468 noted that this morphology is similar to the morphology of the above prepared
469 $Ti_3C_2T_x$. Besides elements Ti and C, no element Al is found in the final product,
470 which suggests that Al layers in Ti_3AlC_2 have been completely etched during the 24 h
471 electrochemical etching process.

472 Based on these results, we then try to *in-situ* synthesize layered TiC_x from
473 $TiO_2/Al_2O_3/C$ precursor ($2TiO_2/0.5Al_2O_3/C$ was used as precursor in this work). The
474 electrosynthesis of Ti_3AlC_2 was firstly carried out at 900 °C and 3.2 V between the
475 $2TiO_2/0.5Al_2O_3/C$ cathode and the graphite anode. After Ti_3AlC_2 was synthesized, the
476 *in-situ* electrochemical etching process was then conducted at 900 °C and 2.5 V
477 between the graphite cathode and the electrosynthesized Ti_3AlC_2 anode, as
478 schematized in Figure 1a. It is evident from the XRD patterns that TiC_x has been
479 successfully prepared from $2TiO_2/0.5Al_2O_3/C$ precursor after 22 h electrolysis and
480 subsequent 24 h electrochemical etching process, as shown in Figure 15a. As same as
481 the electrosynthesized Ti_3AlC_2 precursor (Figure 15b), the obtained TiC_x particles also
482 interconnect with each other (Figure 15c) due to the sintering process at the
483 experimental temperature. Figure 15d and f show respectively the magnified SEM and
484 TEM images of the obtained TiC_x. It is obvious that the obtained TiC_x possesses a
485 layered microstructure (Figure 15f) and the single-layered TiC_x also consists of

nanometer TiC_x particles (Figure 15d). According to the EDS analysis (Figure 15e), only elements Ti and C coexist in the product. It is suggested that element O is first gradually removed during the electrolysis, and element Al is then etched during the electrochemical etching process. Figure 15g shows the high-resolution transmission electron microscope (HRTEM) image and its corresponding SAED pattern of the obtained TiC_x. These images confirm the obtained TiC_x possesses a cubic crystal structure. The *d* spacings measured from the SAED pattern are 2.472, 2.129 and 2.478 Å for the (1-1-1), (200) and (111) lattice planes, respectively. The calculated *a* parameter from these values is 4.28 Å, which confirms that the obtained TiC_x is a carbon-deficient TiC based on the previous work [50].

4 Conclusions

The $TiO_2/Al_2O_3/C$ mixture precursors (including $3TiO_2/0.5Al_2O_3/1.5C$ and $2TiO_2/0.5Al_2O_3/C$) have been electrochemically reduced to Ti_3AlC_2 in molten $CaCl_2$ at 900 °C and 3.2 V by using the molten salt electrolysis process. The carbon content can significantly influence the electrosynthesized products, and the final products can be controlled to form Ti_3AlC, Ti_2AlC and Ti_3AlC_2 with the increase of initial carbon content. The electrosynthesized Ti_3AlC_2 particles with smooth surfaces possess a typical flake-like microstructure. The electroreduction process can generally be divided into three periods, *i.e.*, the formation of the intermediate compounds (such as $CaTiO_3$, $Ca_{12}Al_{14}O_{33}$ and TiC_mO_n), the reduction of the intermediate compounds, and the formation of Ti_3AlC_2. Ti_3AlC_2-derived 2D carbide $Ti_3C_2T_x$ with loose layered structure have also been prepared by the chemical etching process (immersing in 40 %

HF solutions). In addition, layered TiC_x particles have also been *in-situ* produced from the electrosynthesized Ti_3AlC_2 by using the electrochemical etching process, in which the graphite rod is used as the cathode, and Ti_3AlC_2 pellet is served as the anode. These results suggest that the molten salt electrolysis process has a great potential to be used to produce Ti_3AlC_2 and its derived 2D carbides (TiC_x) from $TiO_2/Al_2O_3/C$ precursor.

Acknowledgements

This work was supported by the National Natural Science Foundation of China (No. 51574164), the National Basic Research Program of China (No. 2014CB643403) and the Science and Technology Commissions of Shanghai Municipality (No. 14JC1491400).

References

1. M. Radovic and M. W. Barsoum, *Am. Ceram. Soc. Bull.*, **92**, 20 (2013).
2. P. Eklund, J. Rosen and P. O. Å. Persson, *J. Phys. D: Appl. Phys.*, **50**, 113001 (2017).
3. Z. M. Sun, *Int. Mater. Rev.*, **56**, 143 (2013).
4. N. V. Tzenov and M. W. Barsoum, *J. Am. Ceram. Soc.*, **83**, 825 (2000).
5. X. H. Wang and Y. C. Zhou, *Acta Mater.*, **50** 3141 (2002).
6. Y. W. Bao, J. X. Chen, X. H. Wang and Y. C. Zhou, *J. Eur. Ceram. Soc.*, **24**, 855 (2004).
7. D. J. Tallman, B. Anasori and M. W. Barsoum, *Mater. Res. Lett.*, **1**, 115 (2013).
8. P. Song, J. Sun, Z. Wang, M. Cui, T. Shen, Y. Li, L. Pang, Y. Zhu, Q. Huang and J.

Lü, *Nucl. Instrum. Meth. B*, **326**, 332 (2014).

9. L. M. Peng, *J. Am. Ceram. Soc.*, **90**, 1312 (2007).

10. A. Zhou, C.-A. Wang, Z. Ge and L. Wu, *J. Mater. Sci. Lett.*, **20**, 1971 (2001).

11. J.-H. Han, S.-S. Hwang, D. Lee and S.-W. Park, *J. Eur. Ceram. Soc.*, **28**, 979 (2008).

12. Y. Zou, Z. Sun, S. Tada and H. Hashimoto, *Scr. Mater.*, **56**, 725 (2007).

13. Y. Zou, Z. Sun, S. Tada and H. Hashimoto, *Scr. Mater.*, **55**, 767 (2006).

14. C. Yang, S. Z. Jin, B. Y. Liang, G. J. Liu and S. S. Jia, *J. Mater. Process. Tech.*, **209**, 871 (2009).

15. Y. Zou, Z. M. Sun, H. Hashimoto and L. Cheng, *J. Alloys Compd.*, **468**, 217 (2009).

16. S.-B. Li, H.-X. Zhai, G.-P. Bei, Y. Zhou and Z.-L. Zhang, *Ceram. Int.*, **33**, 169 (2007).

17. A. Zhou, C.-A. Wang and Y. Huang, *J. Mater. Sci.*, **38**, 3111 (2003).

18. A. M. Abdelkader, *J. Eur. Ceram. Soc.*, **36**, 33 (2016).

19. G. Z. Chen, D. J. Fray and T. W. Farthing, *Nature*, **407**, 361 (2000).

20. K. S. Mohandas, *Min. Proc. Ext. Met.*, **122**, 195 (2013).

21. W. Xiao and D. Wang, *Chem. Soc. Rev.*, **43**, 3215 (2014).

22. A. M. Abdelkader, K. T. Kilby, A. Cox and D. J. Fray, *Chem. Rev.*, **113**, 2863 (2013).

23. H. Yin, W. Xiao, X. Mao, W. Wei, H. Zhu and D. Wang, *Electrochim. Acta*, **102**, 369 (2013).

552 24. X. Zou, K. Zheng, X. Lu, Q. Xu and Z. Zhou, *Faraday Discuss.*, **190**, 53 (2016).
553 25. X. Zou, X. Lu, C. Li and Z. Zhou, *Electrochim. Acta*, **55**, 5173 (2010).
554 26. S. Li, X. Zou, X. Lu, K. Zheng, G. Li, C. Chen, Q. Xu and Z. Zhou, *J.*
555 *Electrochem. Soc.*, **164**, D533 (2017).
556 27. X. Zou, X. Lu, Z. Zhou and C. Li, *Electrochem. Commun.*, **21**, 9 (2012).
557 28. H. Xie, H. Zhang, Y. Zhai, J. Wang and C. Li, *J. Mater. Sci. Technol.*, **25**, 459
558 (2009).
559 29. X. Y. Yan and D. J. Fray, *J. Appl. Electrochem.*, **39**, 1349 (2009).
560 30. A. V. Suzdaltsev, A. P. Khramov, Yu. P. Zaikov, A. A. Pankratov, E. G. Vovkotrub
561 and B. D. Antonov, *J. Electrochem. Soc.*, **164**, H5183 (2017).
562 31. M. Naguib and Y. Gogotsi, *Acc. Chem. Res.*, **48**, 128 (2015).
563 32. B. Anasori, M. R. Lukatskaya and Y. Gogotsi, *Nat. Rev. Mater.*, **2**, 16098 (2017).
564 33. M. Naguib, O. Mashtalir, J. Carle, V. Presser, J. Lu, L. Hultman, Y. Gogotsi and
565 M. W. Barsoum, *ACS Nano*, **6**, 1322 (2012).
566 34. A. Feng, Y. Yu, Y. Wang, F. Jiang, Y. Yu, L. Mi and L. Song, *Mater. Design*, **114**,
567 161 (2017).
568 35. Y. Liu, X. Zhang, S. Dong, Z. Ye and Y. Wei, *J. Mater. Sci.*, **52**, 2200 (2017).
569 36. T. Zhang, L. Pan, H. Tang, F. Du, Y. Guo, T. Qiu and J. Yang, *J. Alloys Compd.*,
570 **695**, 818 (2017).
571 37. X. Xie, Y. Xue, L. Li, S. Chen, Y. Nie, W. Ding and Z. Wei, *Nanoscale*, **6**, 11035
572 (2014).
573 38. V. M. Hong Ng, H. Huang, K. Zhou, P. S. Lee, W. Que, J. Z. Xu and L. B. Kong,

574 *J. Mater. Chem. A*, **5**, 3039 (2017).

575 39. X. Xie, S. Chen, W. Ding, Y. Nie and Z. Wei, *Chem. Commun.*, **49**, 10112 (2013).

576 40. M. A. Pietzka and J. C. Schuster, *J. Phase Equilib.*, **15**, 392 (1994).

577 41. X. Wang and Y. Zhou, *J. Mater. Chem.*, **12**, 455 (2002).

578 42. M. Ai, H. Zhai, Y. Zhou, Z. Tang, Z. Huang, Z. Zhang and S. Li, *J. Am. Ceram.*

579 *Soc.*, **89**, 1114 (2006).

580 43. W. Xiao, X. Jin, Y. Deng, D. Wang, X. Hu and G. Z. Chen, *Chemphyschem*, **7**,

581 1750 (2006).

582 44. X. Zou, X. Lu, Z. Zhou, W. Xiao, Q. Zhong, C. Li and W. Ding, *J. Mater. Chem.*

583 *A*, **2**, 7421 (2014).

584 45. S. Li, X. Zou, K. Zheng, X. Lu, Q. Xu, C. Chen and Z. Zhou, *J. Alloys Compd.*,

585 **727**, 1243 (2017).

586 46. B. Jiang, N. Hou, S. Huang, G. Zhou, J. Hou, Z. Cao and H. Zhu, *J. Solid State*

587 *Chem.*, **204**, 1 (2013).

588 47. A. Afir, M. Achour and N. Saoula, *J. Alloys Compd.*, **288**, 124 (1999).

589 48. L. Zhang, S. Wang, S. Jiao, K. Huang and H. Zhu, *Electrochim. Acta*, **75**, 357

590 (2012).

591 49. D. Tang, W. Xiao, L. Tian and D. Wang, *J. Electrochem. Soc.*, **160**, F1192 (2013).

592 50. Y.-F. Yang, H.-Y. Wang, J.-G. Wang and Q.-C. Jiang, *J. Am. Ceram. Soc.*, **91**,

593 3813 (2008).

594 51. Y.-F. Yang, H.-Y. Wang, J. Zhang, R.-Y. Zhao, Y.-H. Liang and Q.-C. Jiang, *J. Am.*

595 *Ceram. Soc.*, **91**, 2736 (2008).

52. C. Peng, C.-A. Wang, Y. Song and Y. Huang, *Mater. Sci. Eng. A*, **428**, 54 (2006).

53. E. H. Kisi, E. Wu, J. S. Zobec, J. S. Forrester and D. P. Riley, *J. Am. Ceram. Soc.*, **90**, 1912 (2007).

54. Y. C. Zhou, J. X. Chen and J. Y. Wang, *Acta Mater.*, **54**, 1317 (2006).

55. T. Yang, C. Wang, C. A. Taylor, X. Huang, Q. Huang, F. Li, L. Shen, X. Zhou, J. Xue, S. Yan and Y. Wang, *Acta Mater.*, **65**, 351 (2014).

56. M. Naguib, M. Kurtoglu, V. Presser, J. Lu, J. Niu, M. Heon, L. Hultman, Y. Gogotsi and M. W. Barsoum, *Adv. Mater.*, **23**, 4248 (2011).

57. F. Chang, C. Li, J. Yang, H. Tang and M. Xue, *Mater. Lett.*, **109**, 295 (2013).

58. M. Bugnet, V. Mauchamp, P. Eklund, M. Jaouen and T. Cabioc'h, *Acta Mater.*, **61**, 7348 (2013).

59. X. Zou, X. Lu, Z. Zhou, C. Li and W. Ding, *Electrochim. Acta*, **56**, 8430 (2011).

60. V. Presser, M. Naguib, L. Chaput, A. Togo, G. Hug and M. W. Barsoum, *J. Raman Spectrosc.*, **43**, 168 (2012).

61. L. Wang, H. Zhang, B. Wang, C. Shen, C. Zhang, Q. Hu, A. Zhou and B. Liu, *Electron. Mater. Lett.*, **12**, 702 (2016).

62. Y. Deng, D. Wang, W. Xiao, X. Jin, X. Hu and G. Z. Chen, *J. Phys. Chem. B*, **109**, 14043 (2005).

63. R. O. Suzuki, M. Aizawa and K. Ono, *J. Alloys Compd.*, **288**, 173 (1999).

64. R. O. Suzuki, K. Ono and K. Teranuma, *Metall. Mater. Trans. B*, **34**, 287 (2003).

65. K. Ono and R. O. Suzuki, *JOM*, **54**, 59 (2002).

66. R. O. Suzuki and S. Inoue, *Metall. Mater. Trans. B*, **34**, 277 (2003).

67. X. Li, C. Zeng and G. Fan, *Int. J. Hydrogen Energy*, **40**, 3883 (2015).

68. P. Yan, R. Zhang, J. Jia, C. Wu, A. Zhou, J. Xu and X. Zhang, *J. Power Sources*, **284**, 38 (2015).

69. X. Li, G. Fan and C. Zeng, *Int. J. Hydrogen Energy*, **39**, 14927 (2014).

70. K. Wang, Y. Zhou, W. Xu, D. Huang, Z. Wang and M. Hong, *Ceram. Int.*, **42**, 8419 (2016).

Table and Figure captions

Table 1. Summary of the phase constitutions of the products electrosynthesized from $TiO_2/Al_2O_3/C$ precursors with different compositions.

Composition (wt %)			Stoichiometry	Main phases	Impurity phases
TiO_2	Al_2O_3	C	Ti:Al:C		
81.8	17.4	0.8	3:1:0.2	Ti_3AlC(s)	Ti_3Al(w)
81.1	17.3	1.6	3:1:0.4	Ti_2AlC (s)	Ti_3AlC(m), TiC(m), Ti_3Al(vw)
80.5	17.1	2.4	3:1:0.6	Ti_2AlC (s)	Ti_3AlC(w), TiC(w), Ti_3Al(vw)
79.8	17.0	3.2	3:1:0.8	Ti_2AlC (s)	Ti_3AlC(vw), TiC(vw), Ti_3Al(vw)
79.2	16.8	4.0	3:1:1.0	Ti_3AlC_2(s)	Ti_2AlC(vw), TiC(vw), Ti_3Al(vw)
78.6	16.7	4.7	3:1:1.2	Ti_3AlC_2(s)	TiC(vw), Ti_3Al(vw)
77.6	16.5	5.9	3:1:1.5	Ti_3AlC_2(s)	TiC(vw)
76.2	16.2	7.6	3:1:2.0	Ti_3AlC_2(s), $TiAl_3$(s), TiC(s)	– – –

*legend for symbols is as follows: “s” = strong; “m” = medium; “w” = weak; and “vw” = very weak.

Figure 1. Schematic illustrations of (a) the etching process and (b) the etching mechanism for Ti_3AlC_2 by the chemical etching process and electrochemical etching process, respectively.

Figure 2. The current-time curve of the electroreduction of $3TiO_2/0.5Al_2O_3/1.5C$ precursor at 900 °C and 3.2 V in molten $CaCl_2$.

Figure 3. XRD patterns of the products obtained from $3TiO_2/0.5Al_2O_3/1.5C$ pellet

after being electrolyzed for 0 (*i*), 1 (*ii*), 2.5 (*iii*), 5 (*iv*), 7.5 (*v*), 10 (*vi*), and 22 h (*vii*), respectively.

Figure 4. (a), (b) Detailed XRD peaks of TiC_mO_n formed after various electrolysis times, and (c) variations of the lattice parameter of TiC_mO_n with the increase of electrolysis time.

Figure 5. XRD patterns of the partially reduced $3TiO_2/0.5Al_2O_3/1.5C$ pellet (electrolyzed for (a) 2 h and (b) 5 h) from the pellet's surface to its center in a certain distance (around 0.3 mm) along the axial direction; (c) is the details of XRD patterns in (b).

Figure 6. (a), (b) SEM images and (c) TEM image of the product obtained from $3TiO_2/0.5Al_2O_3/1.5C$ pellet after 22 h electrolysis; (d) HRTEM image and its corresponding SAED pattern of the electrosynthesized Ti_3AlC_2.

Figure 7. The current-time curve of the electroreduction of $2TiO_2/0.5Al_2O_3/C$ precursor (black line) and $3TiO_2/0.5Al_2O_3/1.5C$ precursor (gray line, for a comparison) at 900 °C and 3.2 V in molten $CaCl_2$.

Figure 8. XRD patterns of the products obtained from the $2TiO_2/0.5Al_2O_3/C$ pellet electrolyzed for 0 (*i*), 4 (*ii*), 8 (*iii*), 12 (*iv*), 16 (*v*) and 22 h (*vi*), respectively.

Figure 9. Variations of the lattice parameter of TiC_mO_n with the increase of electrolysis time during the electroreduction of $2TiO_2/0.5Al_2O_3/C$ precursor.

Figure 10. Raman spectrum of the electrosynthesized Ti_3AlC_2 obtained from the $2TiO_2/0.5Al_2O_3/C$ precursor (after 22 h electrolysis).

Figure 11. (a) Backscattered electron (BSE) image of the section of the partially reduced $2TiO_2/0.5Al_2O_3/C$ pellet (electrolyzed for 8 h) and (b)–(f) the element maps of the corresponding area marked in (a); (g) schematic illustration of the electroreduction of the pellet from the pellet's surface to its center.

Figure 12. SEM images and their corresponding EDS spectra of the products obtained from $2TiO_2/0.5Al_2O_3/C$ pellet electrolyzed for (a) 4 and (b) 22 h, respectively.

Figure 13. (a) XRD patterns of the electrosynthesized Ti_3AlC_2 before and after being immersed in HF solutions for 24 h; (b) SEM image and its corresponding EDS spectrum, (c) FTIR spectrum of the obtained $Ti_3C_2T_x$; (d) TEM image and its corresponding SAED pattern of the obtained $Ti_3C_2T_x$.

Figure 14. (a) XRD patterns of the commercial Ti_3AlC_2 before and after being electrochemically etched at 900 °C and 2.5 V for 24 h in molten $CaCl_2$; SEM images

698 of the commercial Ti_3AlC_2 (b) before and (c) after being electrochemically etched for
699 24 h, the inset in (c) is the corresponding EDS spectrum measured over the SEM
700 image area; (d) is the detailed area marked in (c).
701
702 Figure 15. (a) XRD patterns of the Ti_3AlC_2 electrosynthesized from $TiO_2/Al_2O_3/C$
703 precursor before and after being electrochemically etched for 24 h; SEM images of
704 the electrosynthesized Ti_3AlC_2 (b) before and (c), (d) after being electrochemically
705 etched for 24 h; (e) the corresponding EDS spectrum measured over the SEM image
706 in (d); (f) TEM image as well as (g) HRTEM image and its corresponding SAED
707 pattern of the obtained TiC_x prepared from the electrosynthesized Ti_3AlC_2.

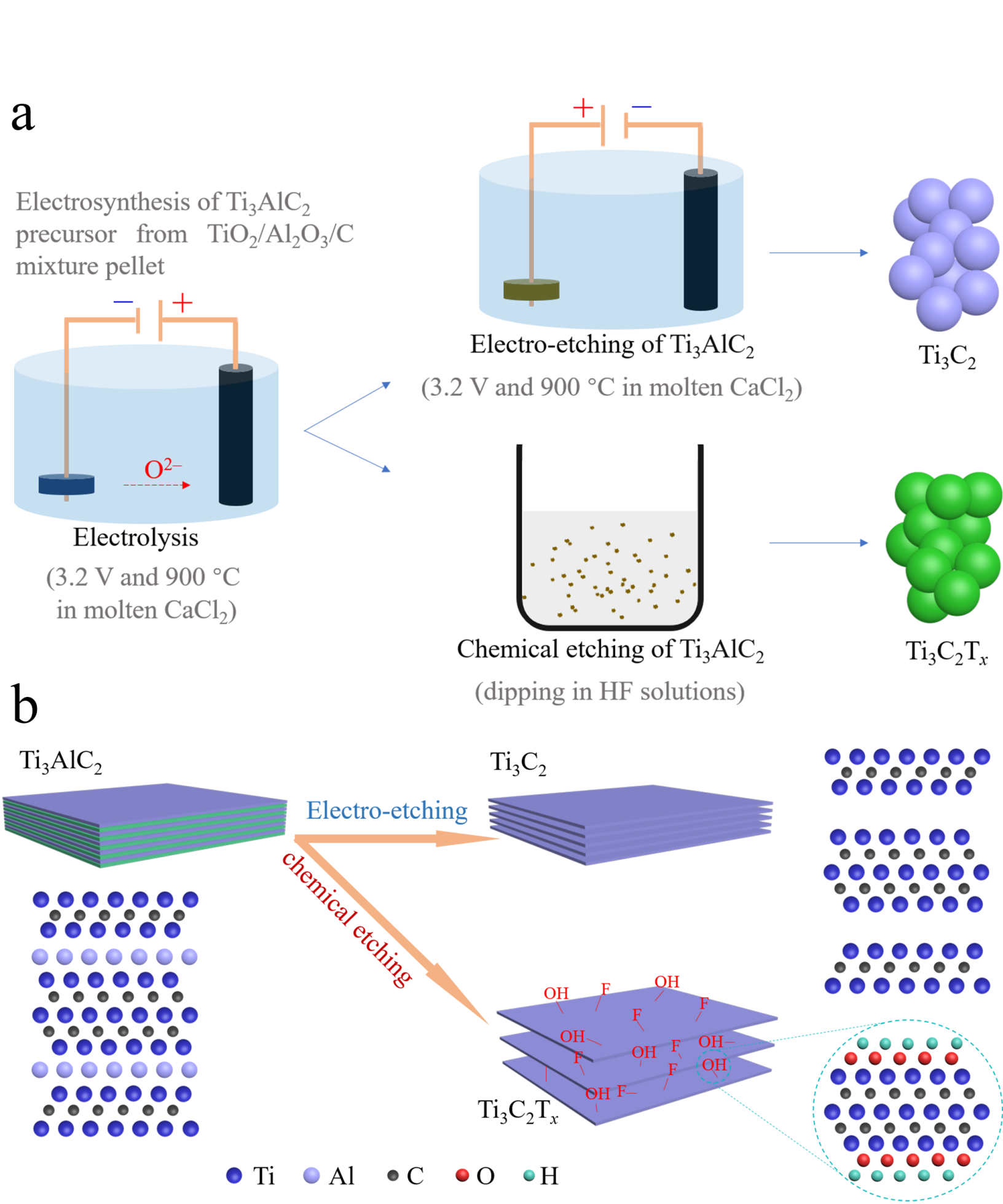
a
Electrosynthesis of Ti_3AlC_2 precursor from $TiO_2/Al_2O_3/C$ mixture pellet
Electrolysis
(3.2 V and 900 °C in molten $CaCl_2$)
O^{2-}
Electro-etching of Ti_3AlC_2
(3.2 V and 900 °C in molten $CaCl_2$)
Ti_3C_2
Chemical etching of Ti_3AlC_2
(dipping in HF solutions)
$Ti_3C_2T_x$
b
Ti_3AlC_2
Ti_3C_2
Electro-etching
chemical etching
OH
F
$Ti_3C_2T_x$
Ti
Al
C
O
H

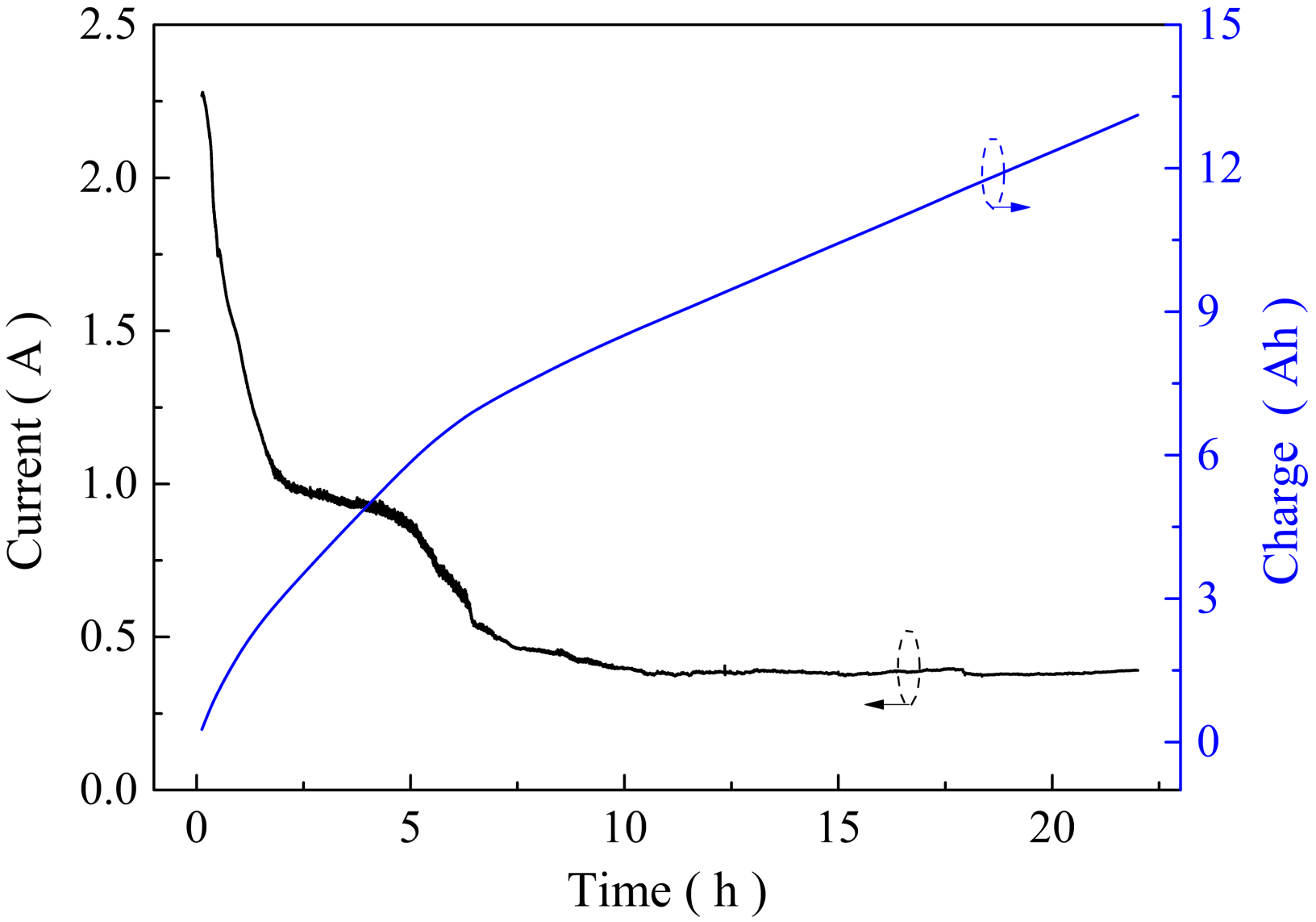
2.5
2.0
1.5
1.0
0.5
0.0
Current (A)
0
5
10
15
20
Time (h)
15
12
9
6
3
0
Charge (Ah)

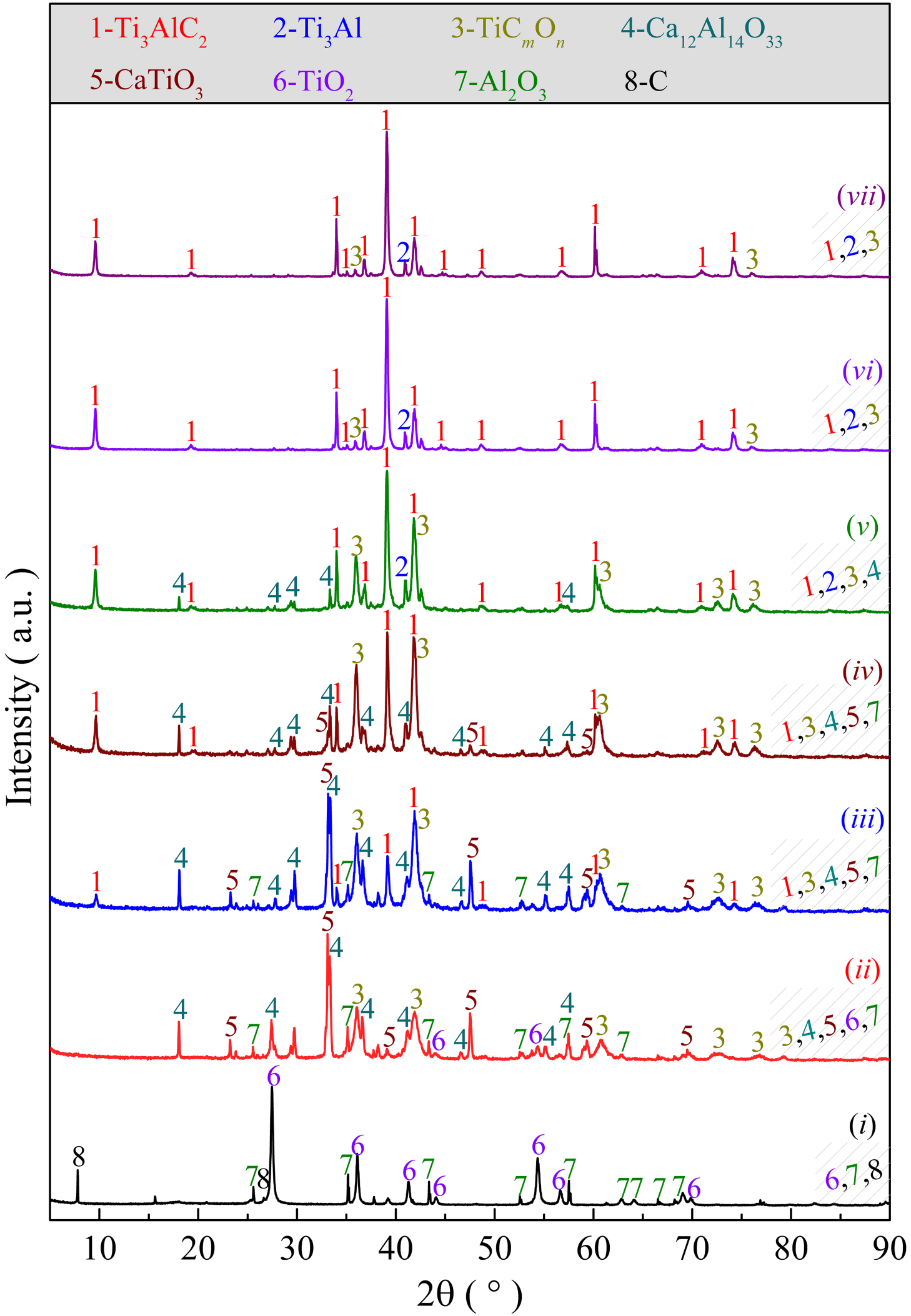
1-Ti3AlC2
2-Ti3Al
3-TiCmOn
4-Ca12Al14O33
5-CaTiO3
6-TiO2
7-Al2O3
8-C
(vii)
(vi)
(v)
(iv)
(iii)
(ii)
(i)
Intensity (a.u.)
2θ (°)
10
20
30
40
50
60
70
80
90

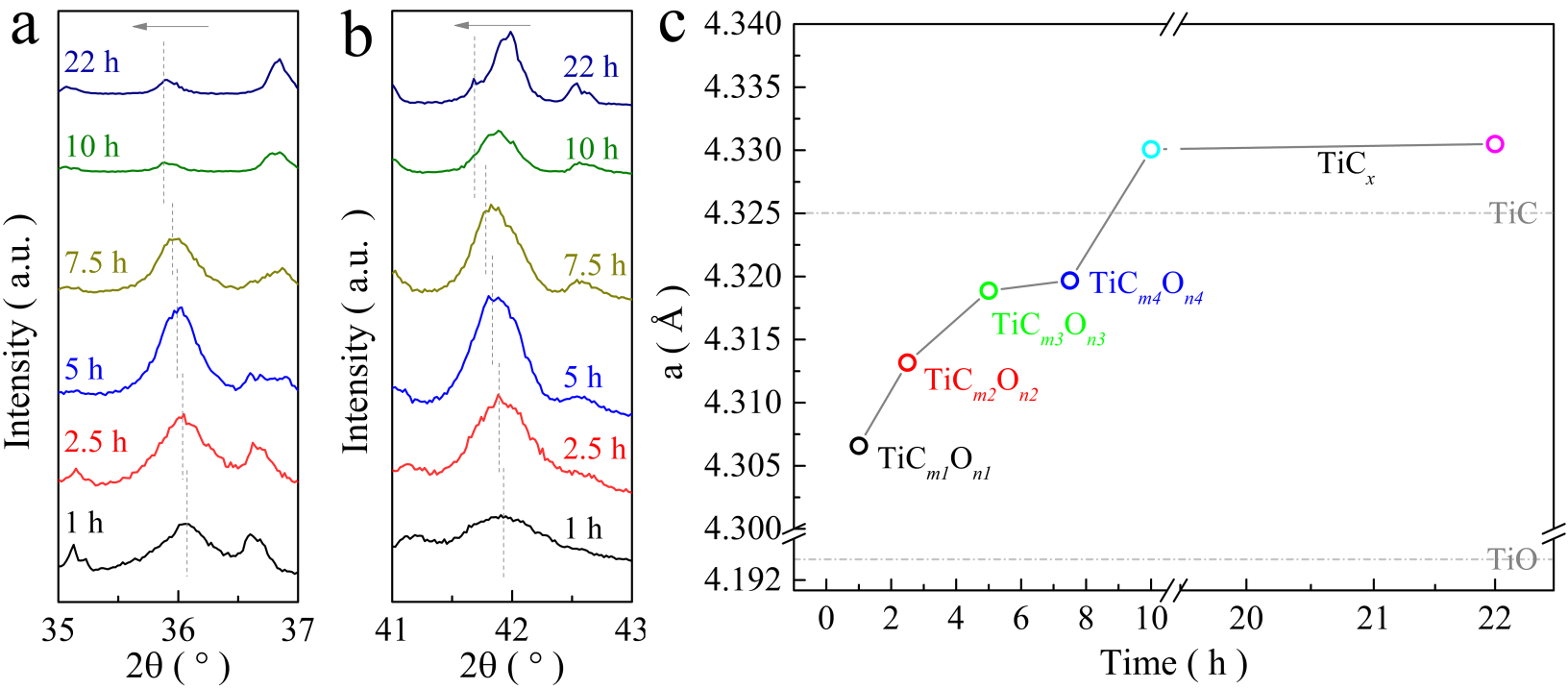
a
22 h
10 h
7.5 h
5 h
2.5 h
1 h
Intensity (a.u.)
35
36
37
2θ (°)
b
22 h
10 h
7.5 h
5 h
2.5 h
1 h
Intensity (a.u.)
41
42
43
2θ (°)
c
4.340
4.335
4.330
4.325
4.320
4.315
4.310
4.305
4.300
4.192
a (Å)
TiC$_x$
TiC
TiC$_{m4}$O$_{n4}$
TiC$_{m3}$O$_{n3}$
TiC$_{m2}$O$_{n2}$
TiC$_{m1}$O$_{n1}$
TiO
0
2
4
6
8
10
20
21
22
Time (h)

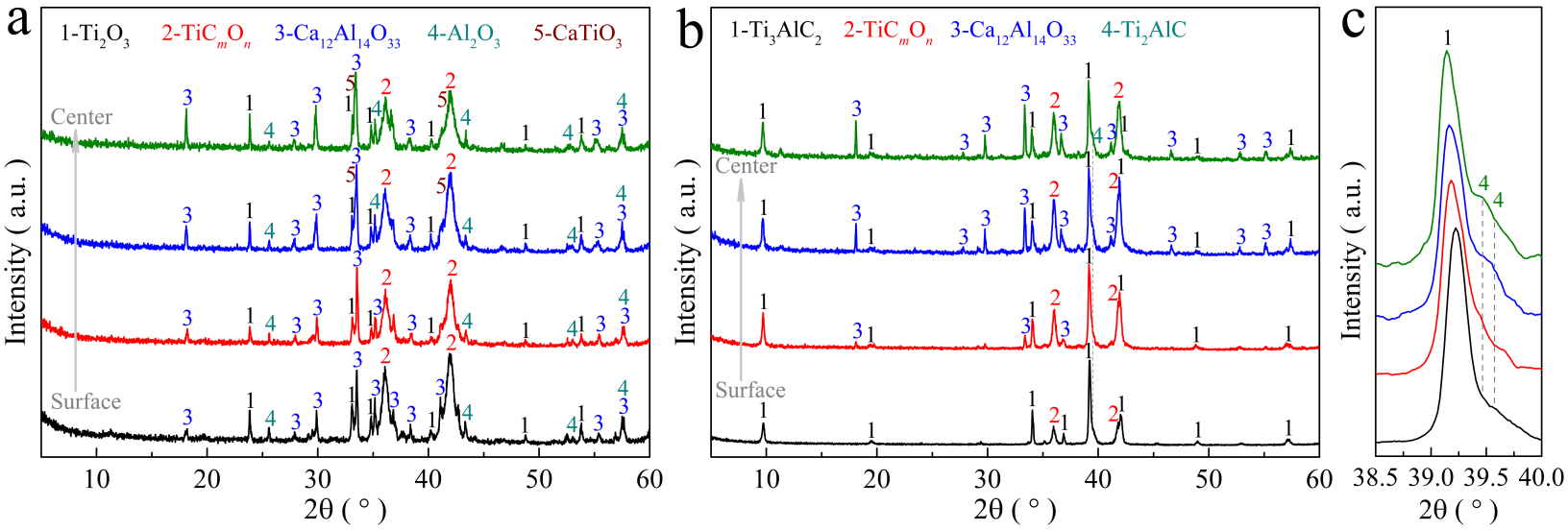
a
1-Ti2O3
2-TiCmOn
3-Ca12Al14O33
4-Al2O3
5-CaTiO3
Center
Surface
Intensity (a.u.)
2θ (°)
b
1-Ti3AlC2
2-TiCmOn
3-Ca12Al14O33
4-Ti2AlC
Center
Surface
Intensity (a.u.)
2θ (°)
c
Intensity (a.u.)
2θ (°)

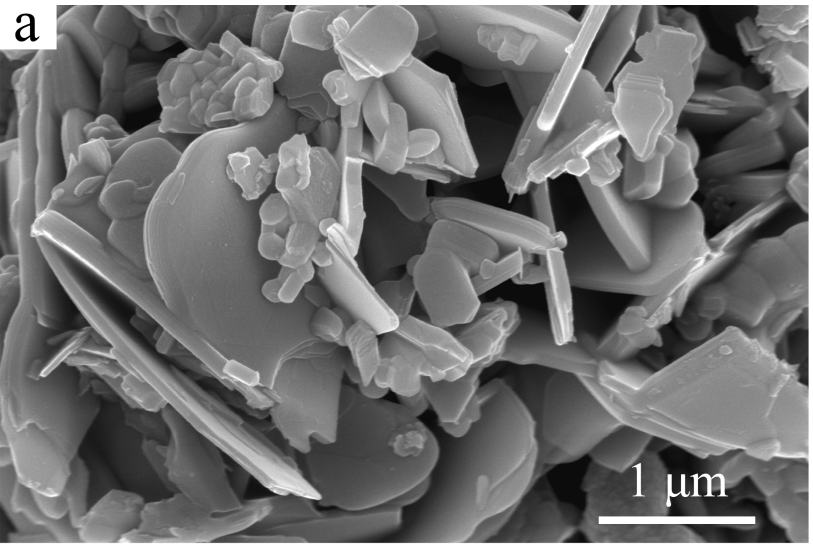
a
1 μm

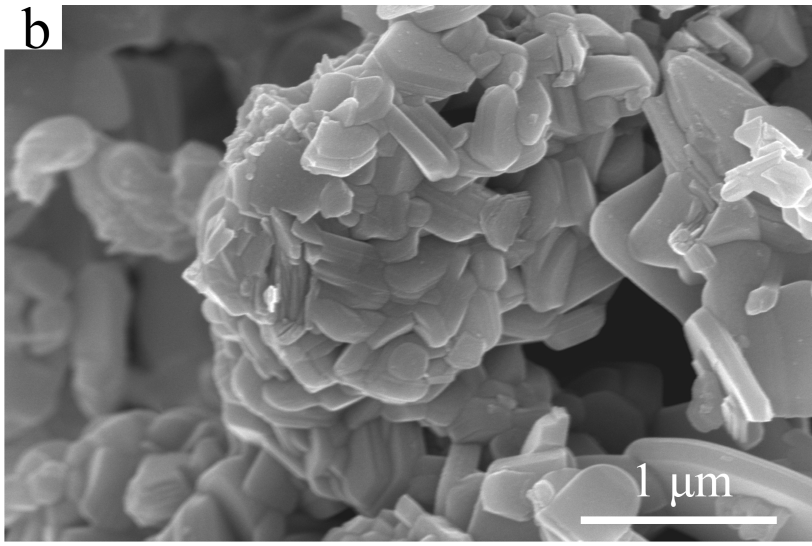
b
1 μm

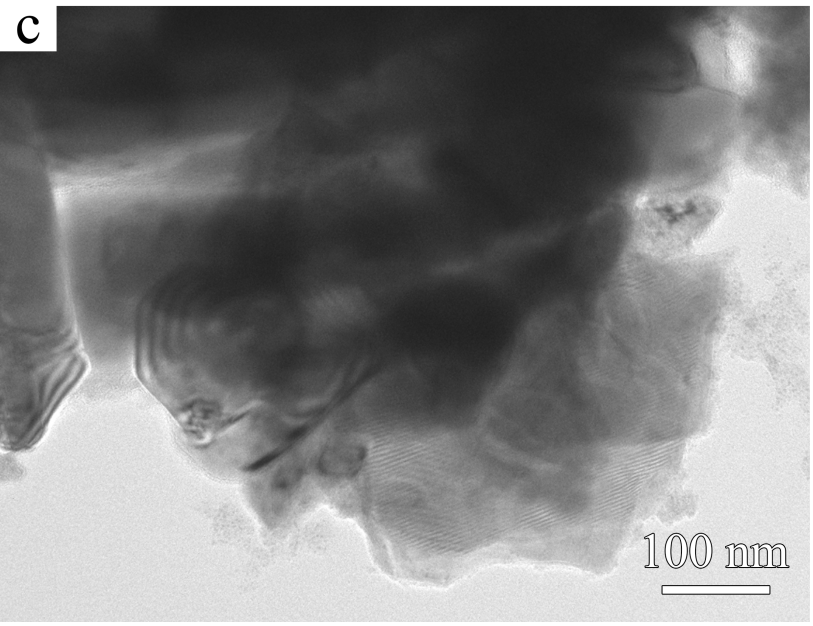
c
100 nm

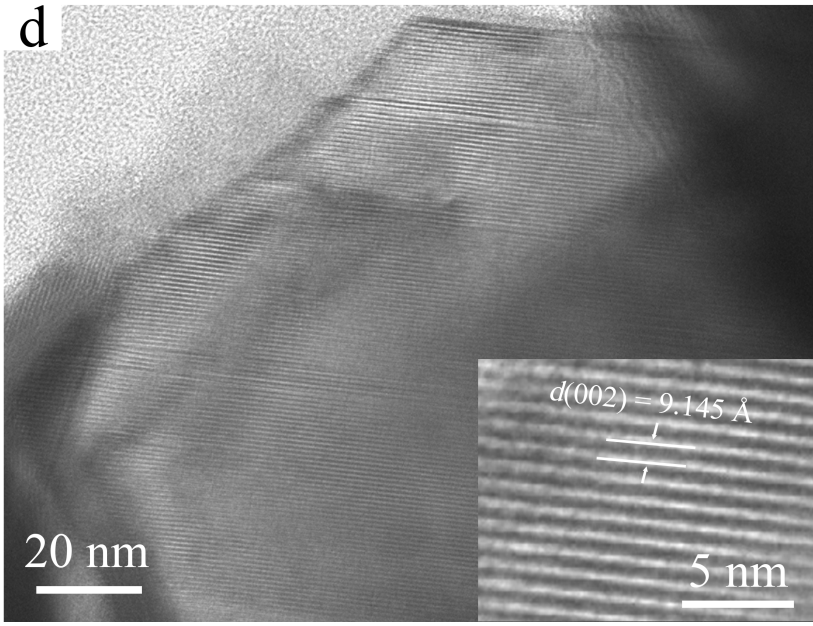
d
20 nm
d(002) = 9.145 Å
5 nm

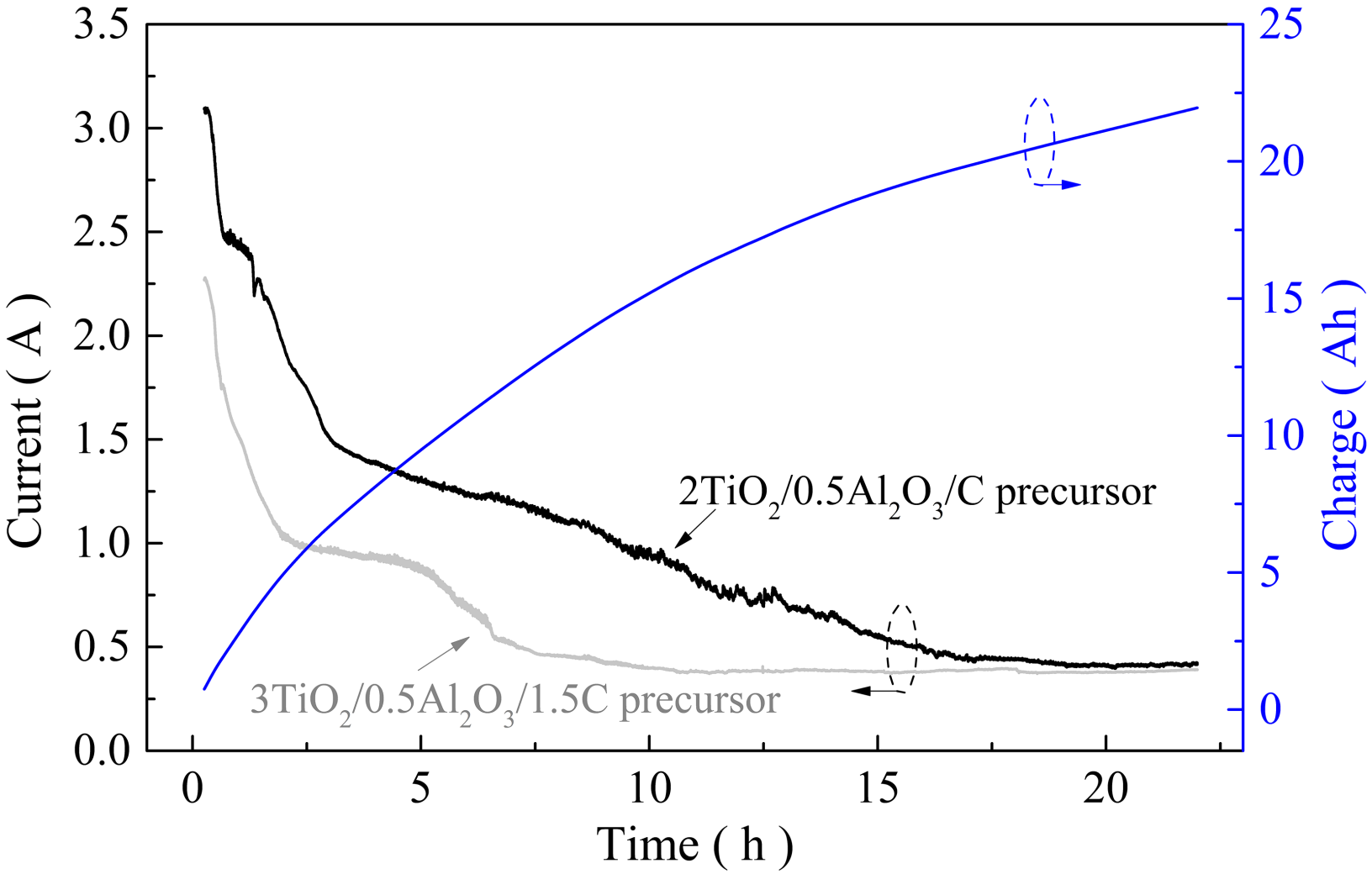
Current (A)
Charge (Ah)
Time (h)
2TiO2/0.5Al2O3/C precursor
3TiO2/0.5Al2O3/1.5C precursor
0.0
0.5
1.0
1.5
2.0
2.5
3.0
3.5
0
5
10
15
20
25

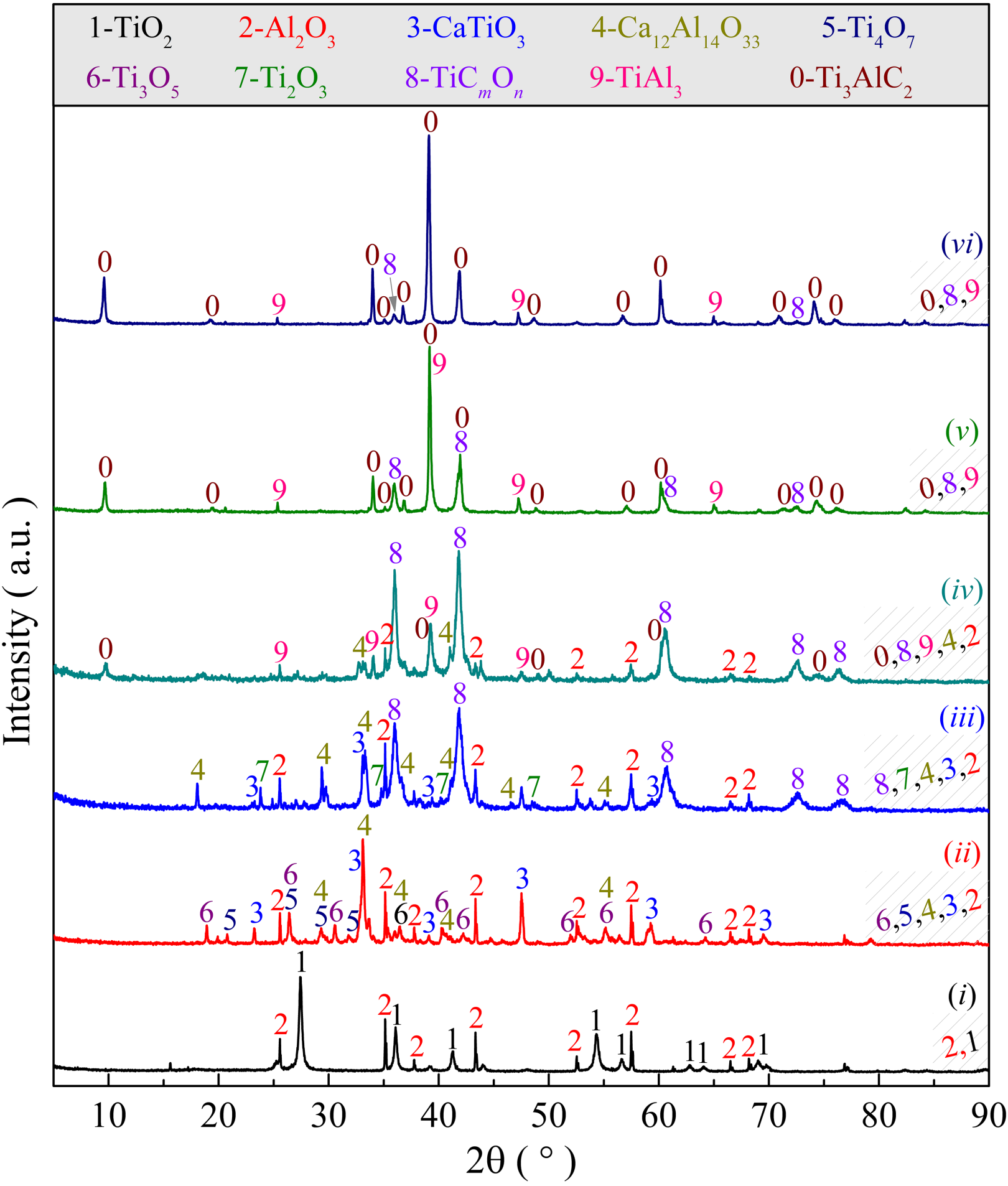
1-TiO2
2-Al2O3
3-CaTiO3
4-Ca12Al14O33
5-Ti4O7
6-Ti3O5
7-Ti2O3
8-TiCmOn
9-TiAl3
0-Ti3AlC2
(vi)
0,8,9
(v)
0,8,9
(iv)
0,8,9,4,2
(iii)
8,7,4,3,2
(ii)
6,5,4,3,2
(i)
2,1
Intensity (a.u.)
10
20
30
40
50
60
70
80
90
2θ (°)

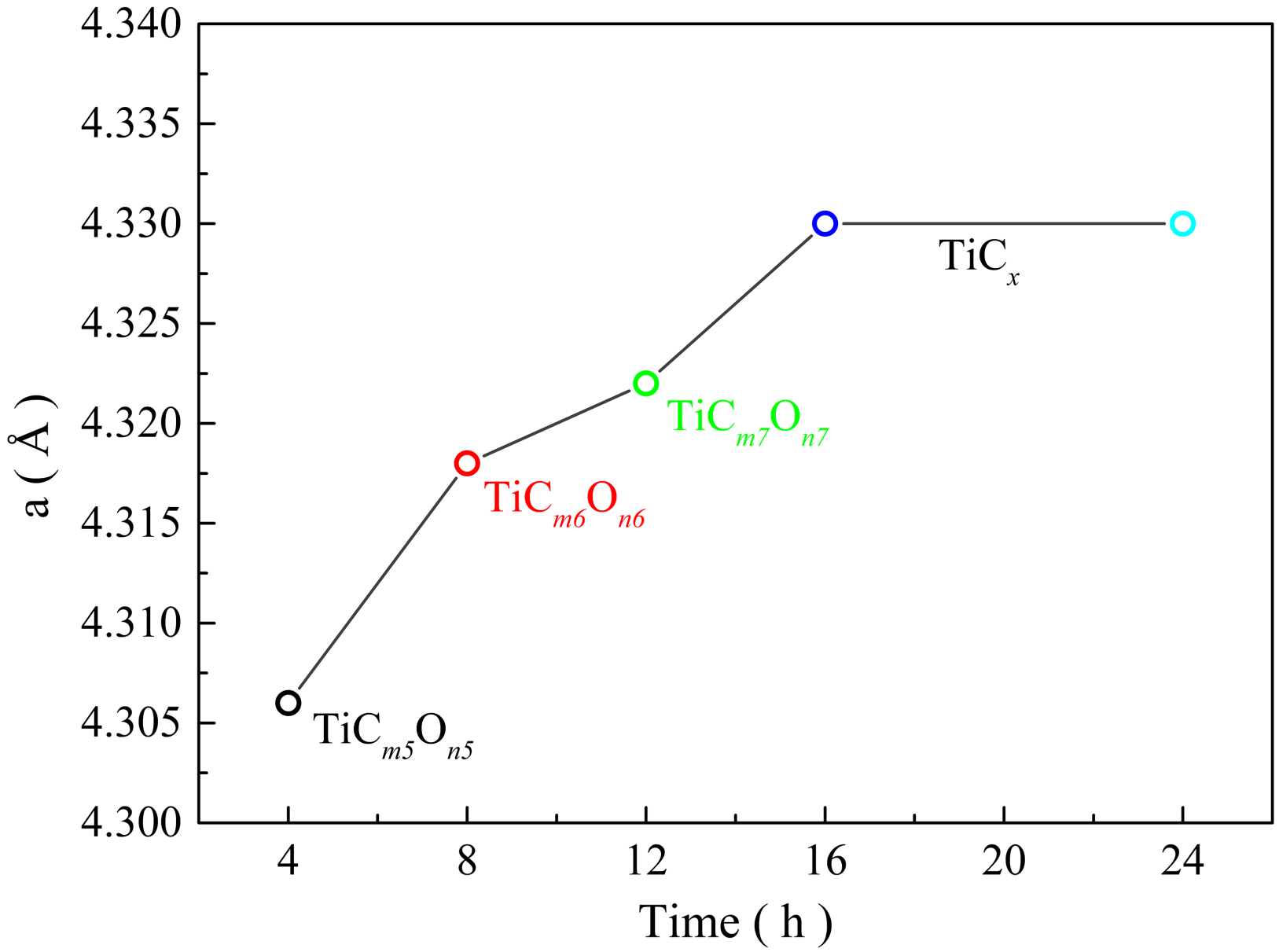
4.340
4.335
4.330
4.325
4.320
4.315
4.310
4.305
4.300
a (Å)
4
8
12
16
20
24
Time (h)
TiC$_{m5}$O$_{n5}$
TiC$_{m6}$O$_{n6}$
TiC$_{m7}$O$_{n7}$
TiC$_{x}$

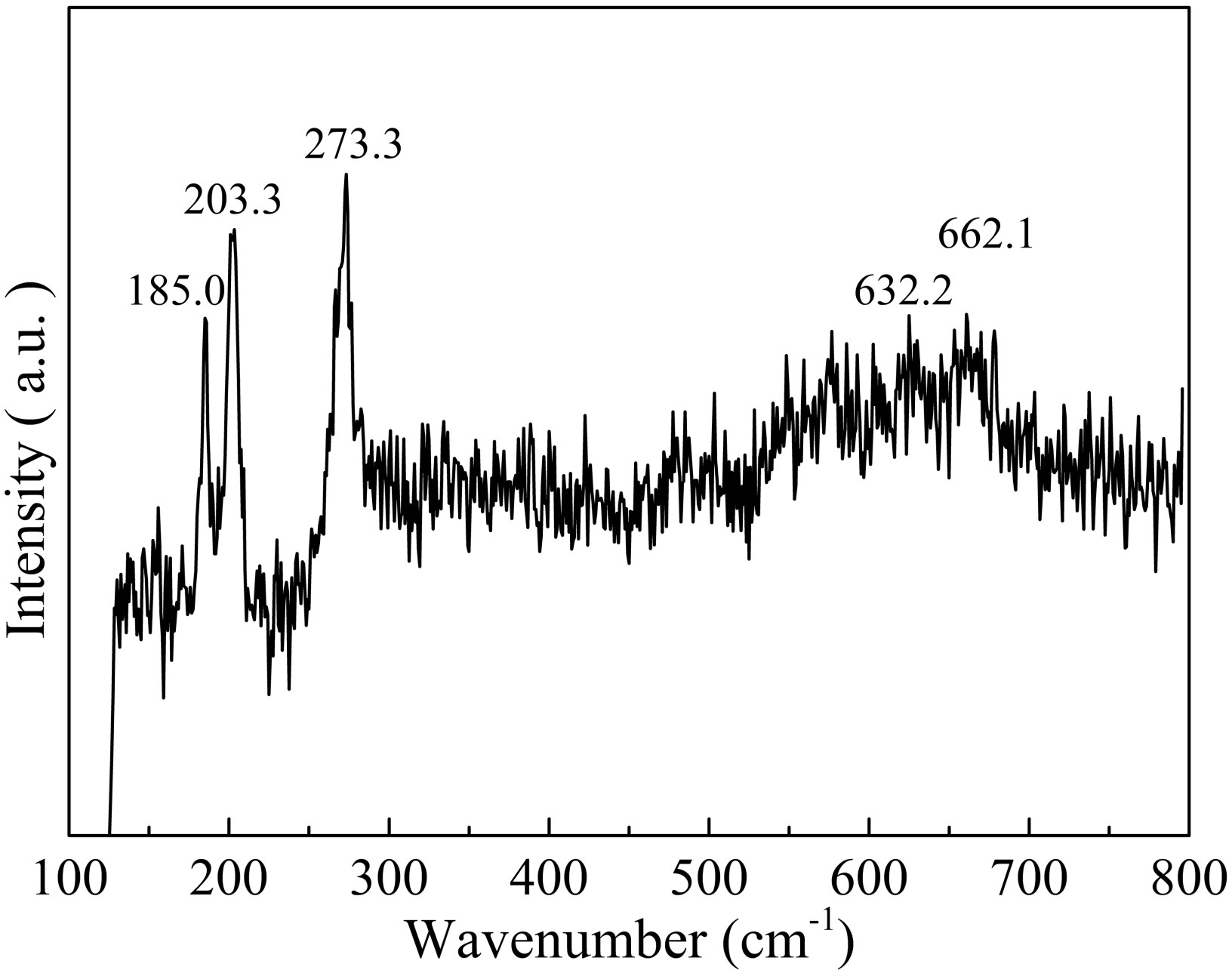
273.3
203.3
185.0
662.1
632.2
Intensity (a.u.)
100
200
300
400
500
600
700
800
Wavenumber (cm-1)

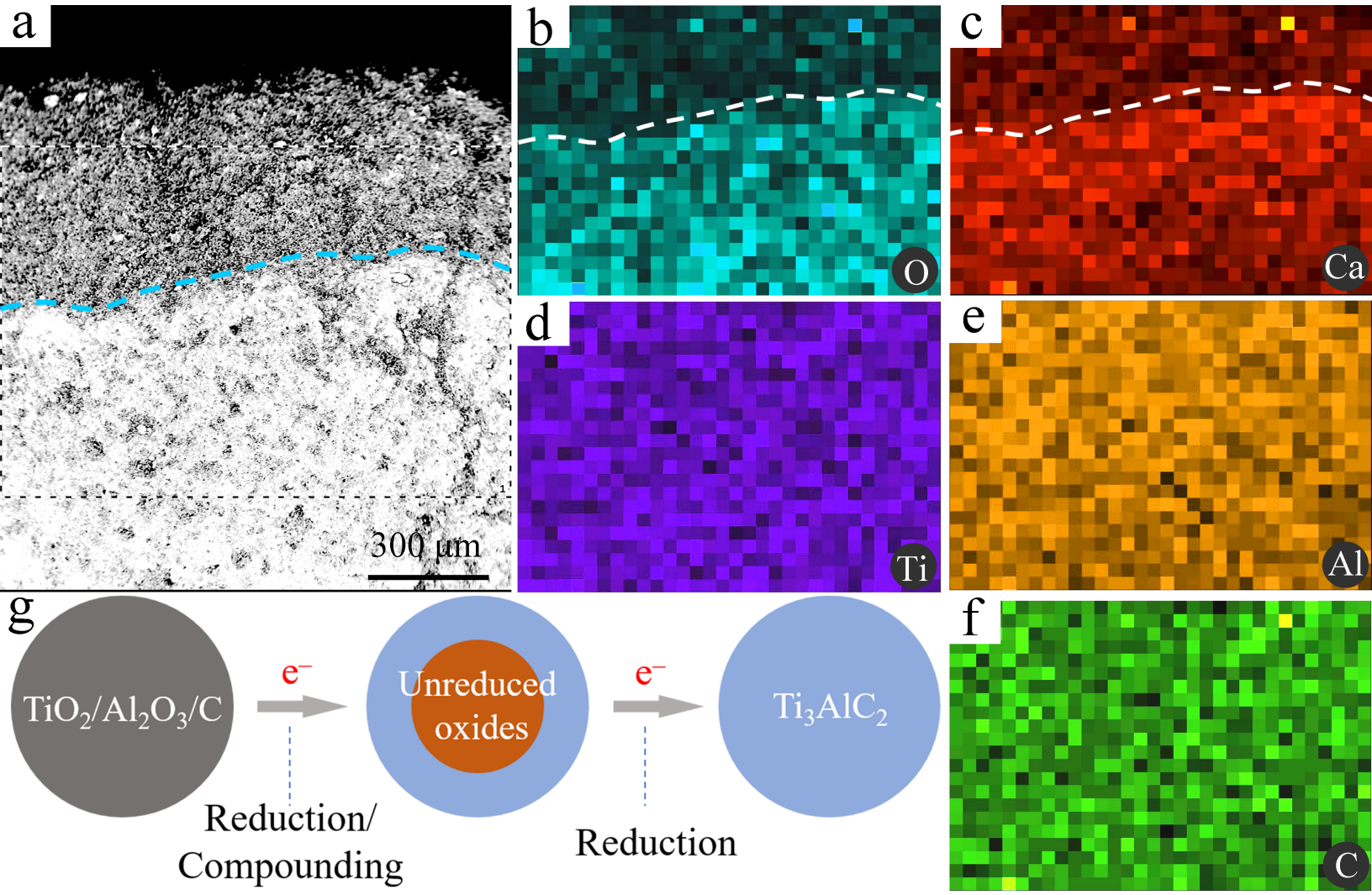
a
300 μm
b
O
c
Ca
d
Ti
e
Al
f
C
g
TiO2/Al2O3/C
e−
Unreduced oxides
e−
Ti3AlC2
Reduction/ Compounding
Reduction

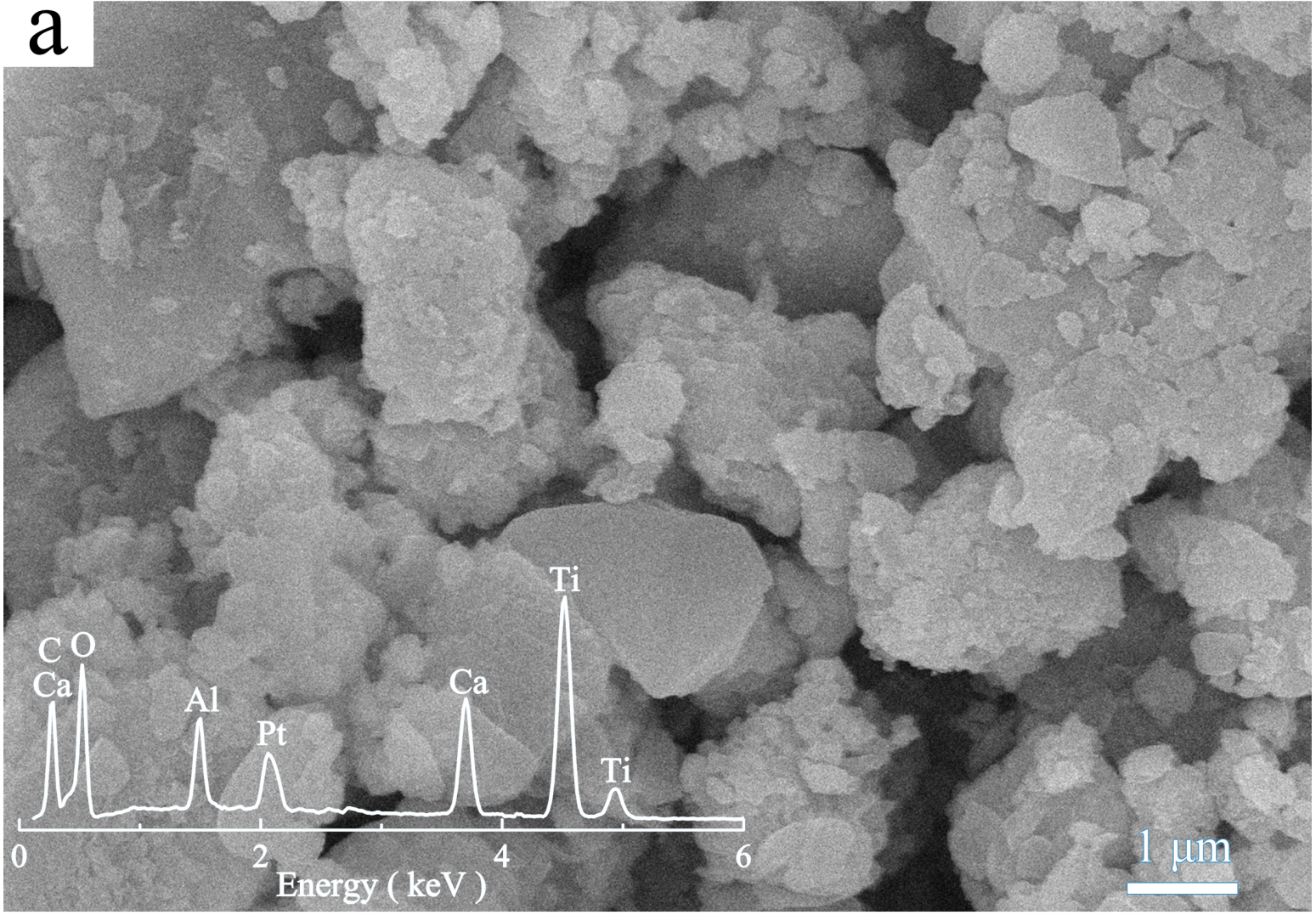
a
C
O
Ca
Al
Pt
Ca
Ti
Ti
0
2
4
6
Energy (keV)
1 μm

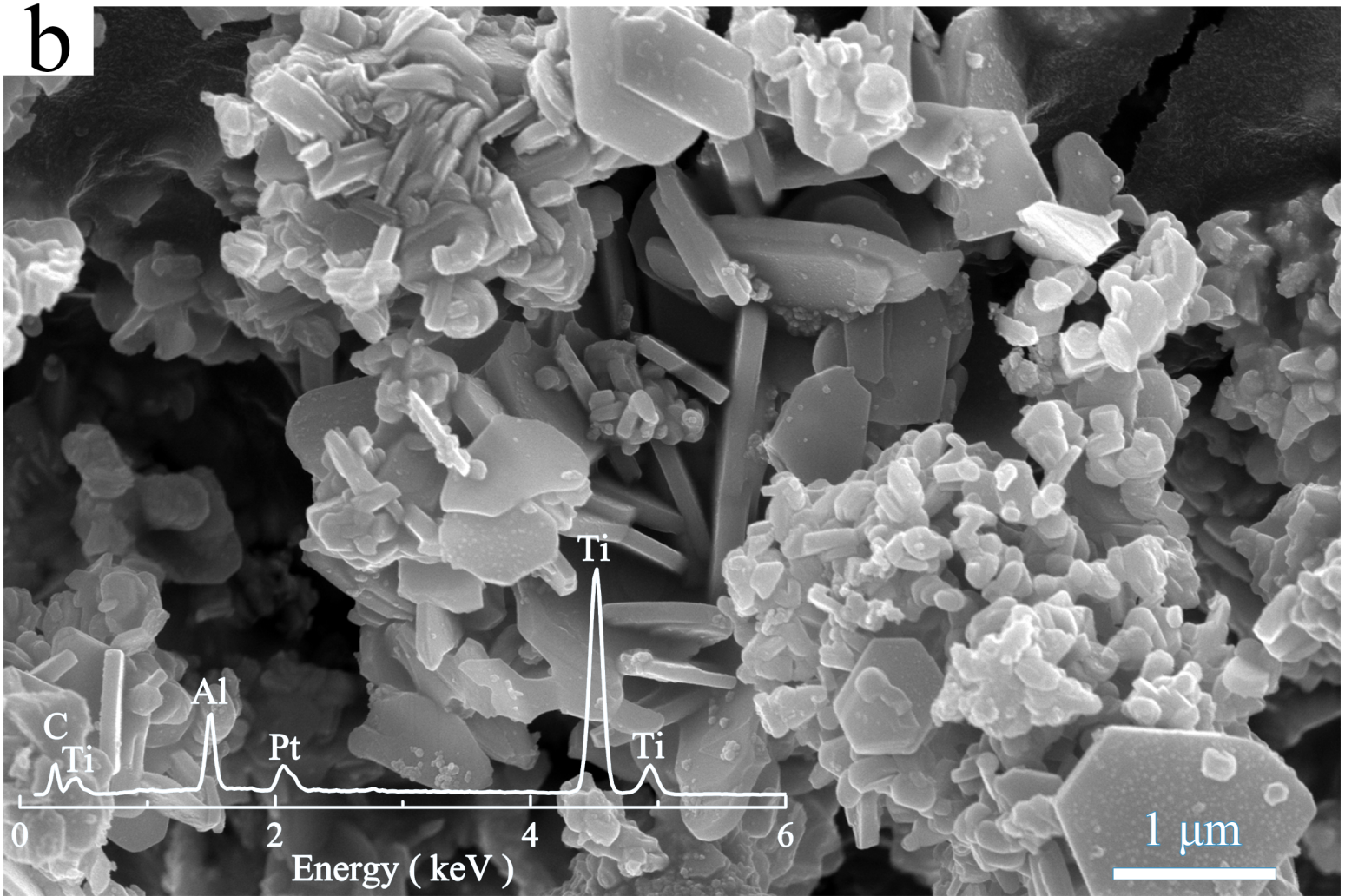
b
Ti
C
Ti
Al
Pt
Ti
0
2
4
6
Energy (keV)
1 μm

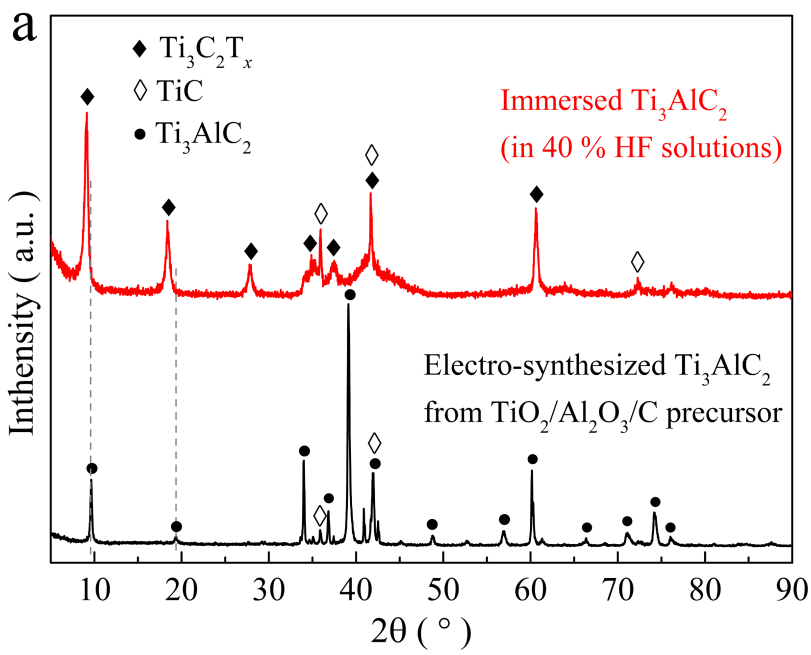
a
♦ Ti3C2Tx
◊ TiC
• Ti3AlC2
Immersed Ti3AlC2
(in 40 % HF solutions)
Electro-synthesized Ti3AlC2
from TiO2/Al2O3/C precursor
Inthensity (a.u.)
10 20 30 40 50 60 70 80 90
2θ (°)

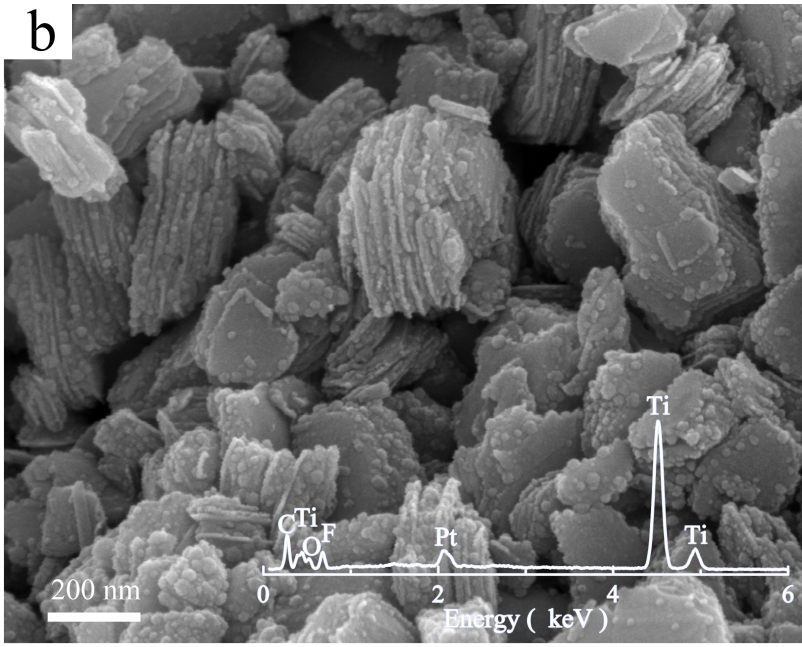
b
C Ti O F Pt Ti
200 nm
0 2 4 6
Energy (keV)

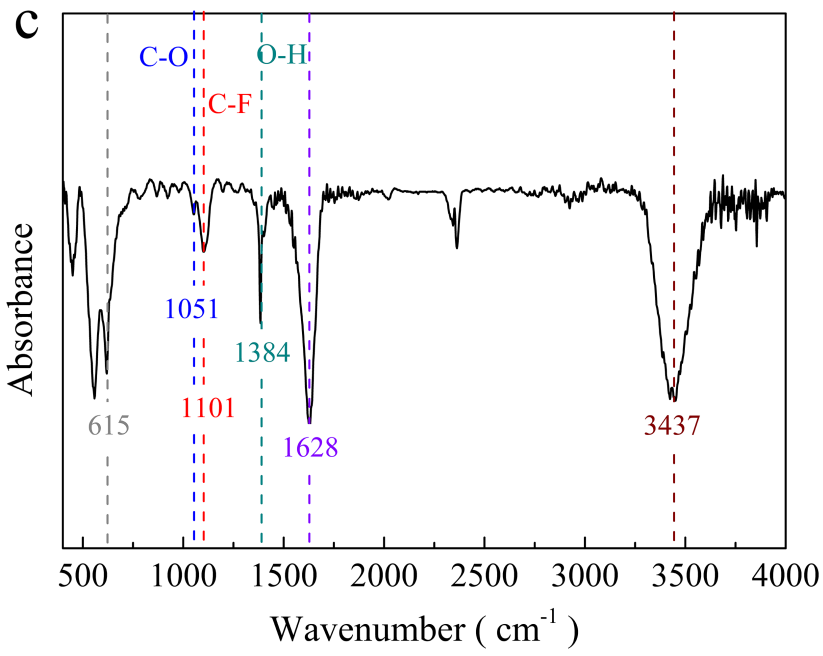
c
C-O
C-F
O-H
1051
1101
1384
615
1628
3437
Absorbance
500 1000 1500 2000 2500 3000 3500 4000
Wavenumber (cm-1)

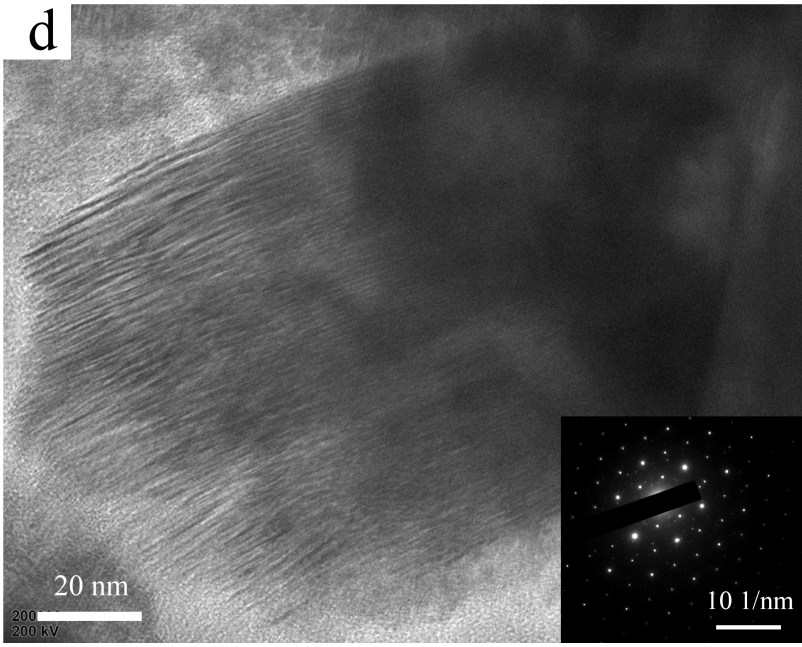
d
20 nm
200
200 kV
10 1/nm

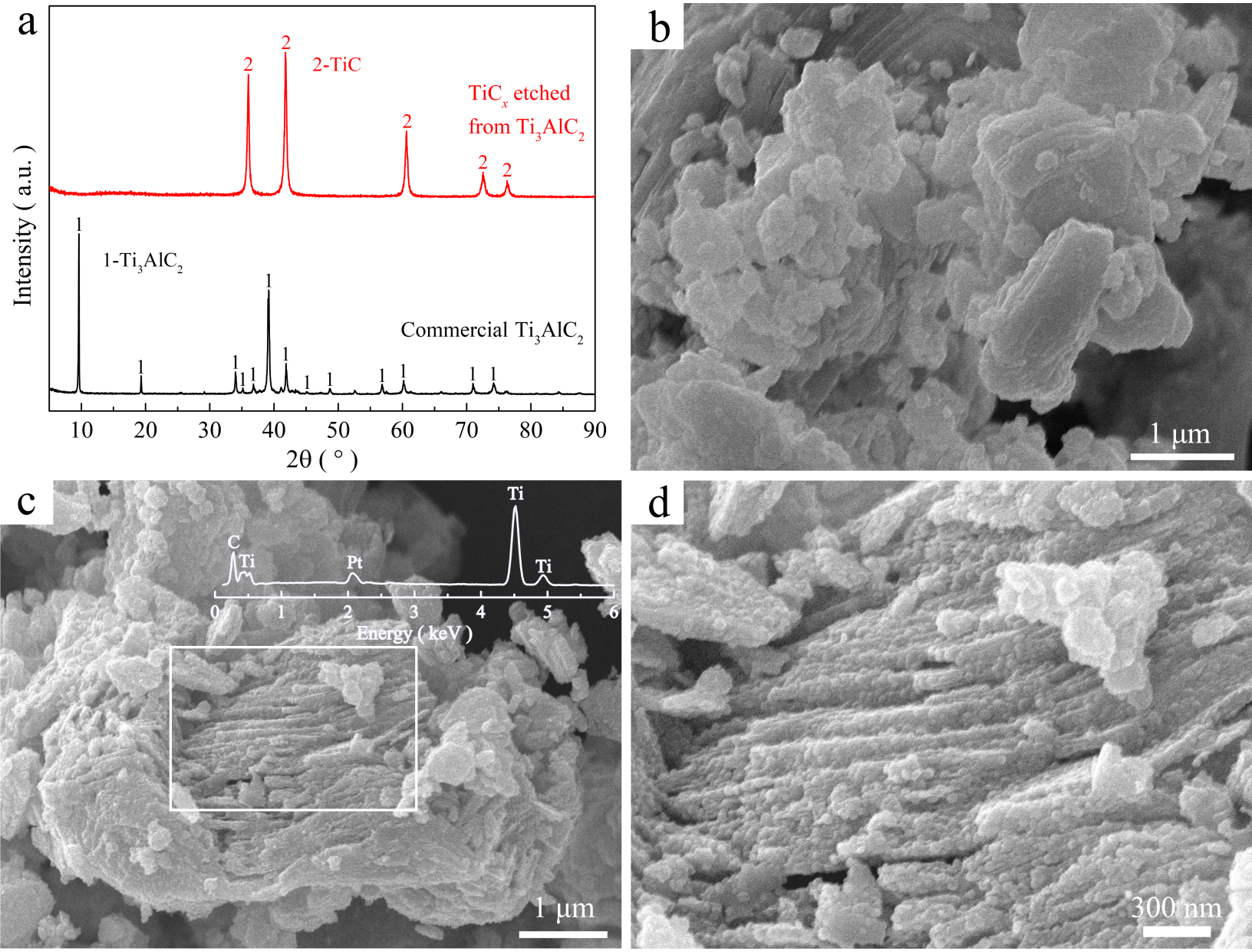
a
2-TiC
TiC$_x$ etched from Ti$_3$AlC$_2$
1-Ti$_3$AlC$_2$
Commercial Ti$_3$AlC$_2$
Intensity (a.u.)
2θ (°)
b
1 μm
c
C
Ti
Pt
Ti
Ti
Energy (keV)
1 μm
d
300 nm

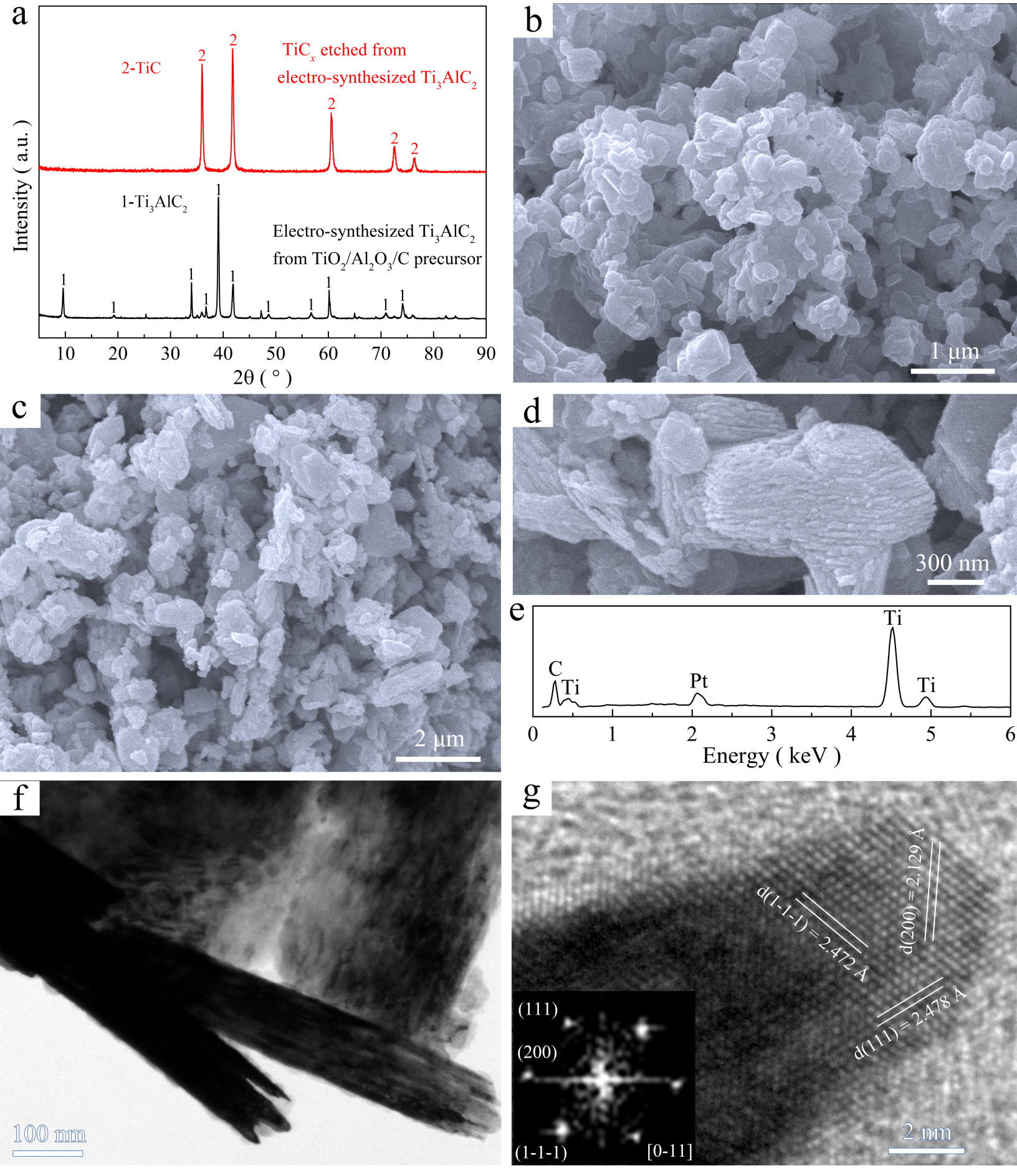
a
2-TiC
TiC$_x$ etched from
electro-synthesized Ti$_3$AlC$_2$
1-Ti$_3$AlC$_2$
Electro-synthesized Ti$_3$AlC$_2$
from TiO$_2$/Al$_2$O$_3$/C precursor
Intensity (a.u.)
2θ (°)
b
1 μm
c
2 μm
d
300 nm
e
C
Ti
Pt
Ti
Ti
Energy (keV)
f
100 nm
g
d(1-1-1) = 2.472 Å
d(200) = 2.129 Å
d(111) = 2.478 Å
(111)
(200)
(1-1-1)
[0-11]
2 nm